THE TRANSPORT COEFFICIENTS IN $(R_{1.5}Ce_{0.5})RuSr_2Cu_2O_{10-\delta}$ (R=Gd, Eu) RUTHENO-CUPRATES

A Thesis

by

MARYNA PETROVNA ANATSKA

Submitted to the Office of Graduate Studies of
Texas A&M University
in partial fulfillment of the requirements for the degree of

MASTER OF SCIENCE

December 2006

Major Subject: Physics

THE TRANSPORT COEFFICIENTS IN $(R_{1.5}Ce_{0.5})RuSr_2Cu_2O_{10-\delta}$ (R=Gd, Eu) RUTHENO-CUPRATES

A Thesis

by

MARYNA PETROVNA ANATSKA

Submitted to the Office of Graduate Studies of
Texas A&M University
in partial fulfillment of the requirements for the degree of

MASTER OF SCIENCE

Approved by:

Chair of Committee,	Glenn Agnolet
Committee Members,	Donald G. Naugle
	Renald Guillemette
Head of Department,	Edward Fry

December 2006

Major Subject: Physics

ABSTRACT

The Transport Coefficients in $(R_{1.5}Ce_{0.5})RuSr_2Cu_2O_{10-\delta}$ (R=Gd, Eu)

Rutheno-Cuprates. (December 2006)

Maryna Petrovna Anatska, B.A., Belarusian State University

Chair of Committee: Dr. Glenn Agnolet

The thermal conductivity, thermopower, and electrical resistivity of $(R_{1.5}Ce_{0.5})RuSr_2Cu_2O_{10-\delta}$ (R=Gd, Eu) polycrystalline samples with different oxygen doping level are investigated in temperature range 1.8-300 K. Much attention is focused on the dependence of the effect of the annealing in high oxygen pressures as well as the effect of aging on transport coefficients in normal and superconducting states. It was found that the process of deoxydation goes faster for Ru-1222(Eu) samples than for Ru-1222(Gd) samples, which results in more pronounced granular effects in Ru-1222(Eu) samples. The relative contribution to the thermal conductivity due to electrons and phonons was estimated by using the Wiedemann-Franz relation and the resistivity data. The calculation showed that the maximum electron contribution for Ru-1222(Eu) is about 0.75% and that for Ru-1222(Gd) samples is around 4 %.

DEDICATION

To my grandma Maria.

ACKNOWLEDGMENTS

First of all I would like to thank Professor Donald G. Naugle for providing the opportunity to be a member of his group at Texas A&M University. I am grateful for his constant encouragement, support, and for the time he spent on valuable discussions.

I am very grateful to Dr. Daya Rathnayaka for his valuable advices and continuous support during my work at the laboratory.

My special thanks go to Dr. Belevtsev and Dr. Krasovitsky for their help and pleasant collaboration.

I am grateful to all of our staff at the Physics Department and members of the Machine and Electronics shop. Especially I would like to thank James Kirby from the Electronics shop for his frequent and professional assistance in finding the electronic components for my project.

I would like to thank all my colleagues and friends at the Physics Department, especially, Dr. Igor Lyuksyutov, Saeed Adegbenro, Aaron DuMar, Esad Ozmetin and Han-gil Lee for their helpful discussions. I thank also members of the advisory committee Dr. Agnolet, Dr. Guillemette, and members of the thesis office at TAMU for providing useful suggestions during the text preparation.

This dissertation would not have been possible without support and inspiration from my parents, my sisters and my husband Nikolai.

TABLE OF CONTENTS

Page

Page

LIST OF FIGURES

Page

Page

Page

LIST OF TABLES

Page

I INTRODUCTION

A. Introduction and Historical Background

It had been known early in the nineteenth century that the resistivity of metallic electrical conductors decreased with temperature. At that time there was no widely accepted theory for the behavior of free electrons in metals. In the absence of data at very low temperatures, two hypotheses were proposed. One suggested that resistivity of a pure metal would be reduced to zero as temperature approached the absolute zero. If a metal has some defects and impurities, the resistivity would tend to a constant value called the residual resistivity. Residual resistivity depends on the amount of the alien atoms (impurities) as well as various other defects in the sample. The fewer is the amount of defects in a sample, the lower is its residual resistivity. The other theory predicted that the metallic resistivity would decrease to a minimum level at low temperatures and then increase dramatically as temperature was lowered still further because conducting electrons would recombine with atoms, which implies an infinite resistivity at T=0. This issue was resolved in the 1911 by the man who first liquefied helium gas, H. Kamerlingh Onnes. While Onnes obviously hoped to settle the argument about which of the current theories best described metallic conduction at low temperatures, he expected to find that one of the common theories of the day would prevail. During his first experiments with platinum wire, he noticed that resistance diminished gradually and than leveled off at 4.3 K [1]. This seemed to fit one of the most

---

This thesis follows the style of *Journal of Physics C*.

widely held theories that such a leveling-off was consistent with impurities. After several experiments, Onnes noticed that the purer the metal, the smaller the residual resistance was. He was just trying to find out how small the residual resistivity could be made by sample purification. Since mercury is liquid at room temperature, it was easy to purify by repeated distillation, Onnes decided to use it for his next experiments. The results were unexpected. The resistance suddenly disappeared below 4.2 K. After repeated experiments with purified mercury, Onnes used the sample of non-purified mercury with supposedly noticeable residual resistance. The results were the same; the resistance disappeared irrespective of sample “purity”.

It was Onnes who not only discovered the superconductivity of pure mercury, tin and lead but was also the first to find superconducting (mercury-gold and mercury-tin) alloys.

It should be mentioned one more property of superconductors discovered by Onnes. Right after discovery of superconductivity, Onnes was interested in applications of superconducting materials for development of intense magnetic fields. Later he learned that small current densities in a sample and quite ordinary levels of magnetic fields destroyed the superconducting state. To explain this phenomenon, Silsbee, a physics assistant at the U.S. National Bureau of Standards, suggested that the disappearance of superconductivity at higher current densities was due to the fact that the superconducting current generates a magnetic field at the surface of the superconductor [1], which destroys the superconducting state.

The second important property of superconductors was discovered in 1933 by W. Meissner and R. Ochsenfeld. They found that superconductors were perfect diamagnets in low applied magnetic fields. When a superconductor is placed in a constant magnetic field, it completely expels magnetic flux from its interior as long as H does not exceed a certain critical value. This demonstration of the perfect diamagnetism in superconductors is known as the Meissner-Ochsenfeld effect.

In 1935, the phenomenological theory of superconductivity was proposed by Heinz and Fritz London to explain the Meissner-Ochsenfeld effect. In general, London theory describes how superconducting currents respond to electric and magnetic fields. If we return to the Meissner-Ochsenfeld experiment, the London theory indicates that even if the superconductor is a perfect diamagnetic, the magnetic field penetrates in a very thin layer near the surface of the superconductor. It is precisely the place where superconducting currents, induced by an external magnetic field, circulate within the superconductor and create magnetic fields that exactly cancel any field applied externally. The London theory shows that the externally applied magnetic field decreases exponentially as it penetrates into the surface of the material. Analyzing experiments, London brothers found that not all of the Maxwell's equations are applicable to describing the behavior of superconducting current in the presence of electromagnetic fields. They found a new relationship between the superconducting current flow and the magnetic field. It does not mean that Maxwell's equations are incorrect; simply that the microscopic description of superconducting current must include not only the interaction with electromagnetic fields (described by Maxwell's

equations) but also the interaction of electrons with the crystal lattice, which affects the response of superconducting current to external fields [1].

Another important development in the thirties was the 1934 Gorter-Casmir theory. According to the Gorter-Casmir theory, the conduction electrons in a superconductor consist of two types, superconducting and normal electrons, with the proportion of superconducting electrons ranging from none at the beginning of the superconducting state to 100% at T=0 K. Still it was unclear what superconducting electrons were.

The greatest advance in understanding the microscopic mechanism of superconductivity came with the discovery of the isotope effect in superconductors. The isotope effect was predicted by H. Froehlich and was discovered experimentally by E. Maxwell and coworkers. They noticed that the temperature of the superconducting transition depends on the average isotopic mass of atoms in the superconductor. The transition temperature T_c for many superconductors is proportional to $1/M^{1/2}$, where M is the mass of the isotope of a particular element. The mass of a particular atom depends on the number of neutrons in its nucleus. Since lattice vibrations depend on the mass of the atom, this suggested that lattice vibrations (phonons) play an important role in superconductivity [2, 3].

The experimental demonstration of the isotope effect pointed the way toward the successful microscopic theory of superconductivity proposed by Bardeen, Cooper, Schrieffer in 1957. This theory explains that superconducting charges in the two-fluid model proposed by Gorter and Casmir are bound electron pairs later called Cooper pairs.

The attraction between two electrons to form a Cooper pair is due to exchange of phonons (lattice vibrations) between them. This interaction is called the electron-phonon interaction. There is the usual Coulomb repulsion between Cooper pairs but at sufficiently low temperatures an attraction between the electrons due to electron-phonon interaction prevails.

1. Second-Order Superconductors

In 1936, the group of L.V. Shubnikov at Kharkov showed that a single crystal of $PbTl_2$ had two distinct critical fields [4]. Up to a lower critical field (Hc_1), the flux of magnetic field is excluded, but above that field the flux begins to penetrate and increases in its penetration until an upper critical field (Hc_2) is reached. Above the upper critical field the flux completely penetrates and superconductivity is extinguished. The superconductors that show this characteristic became known as Type II superconductors. Thus Type II superconductors have a mixed-state above H_{C1} in which the Meissner effect is absent.

On the basis of a phenomenological theory of superconductivity, in 1957, A. A. Abrikosov showed that the existence of mixed-state could be achieved by creating a vortex state [5]. In the mixed-state magnetic vortices are created as a result of the action of the Lorence force on the superconducting electrons, causing Cooper pairs to move in circular motion. The closer the Cooper pair to the axis of rotation, the bigger its angular velocity. By moving in circular motion they create a magnetic field, which screens the

applied field from the remainder of the superconducter. When the superconducting electron reaches the critical value however, the induced magnetic field destroys the Cooper pairs and consequently superconductivity in a region close to the axis of rotation where the applied field can penetrate. Thus the Type II superconducting material has two regions: a superconducting and a non-superconducting core where the external magnetic field penetrates. Vortices appear when the external magnetic field strength reaches the critical value of Hc_1. As the field strengthens, the number of vortices increases and the distance between them decreases. As soon as the external magnetic field reaches the upper critical value of Hc_2, superconductivity disappears completely.

Quantitatively speaking, the difference between Type I and Type II superconductors depends on the relative value of the coherence length and a magnetic penetration depth. The coherence length has to do with the fact that the superconducting electron density cannot change quickly; there is a minimum length over which a given change can be made, lest it destroy the superconducting state. For example, a transition from the superconducting state to a normal state will have a transition layer of finite thickness, which is related to the coherence length. The penetration depth refers to the exponentially decaying externally applied magnetic field at the surface of a superconductor. If the coherence length is longer than the penetration depth, the superconductor will be type I. If the coherence length is shorter than the penetration depth, then the superconductor will be Type II.

In 1986 high temperature superconductors, oxides with T_c above liquid nitrogen temperature were discovered. All high T_c (high critical temperature) superconductors are

Type II superconductors [6]. The complete microscopic theory of high T_c still does not exist. It is known that the supercurrent is created by Cooper pairs but what particles form a Cooper pair and the mechanism for pair formation is unknown.

2. Magnetic Superconductors

Superconductivity can be destroyed by an external magnetic field. Thus we might expect that it could also be destroyed if the magnetic moments of the ions in a crystal magnetically ordered (ferro- or antiferromagnetically) or even if paramagnetic atoms are alloyed into the crystal [6]. A Cooper pair consists of two electrons with opposite spins (at least for most superconducting materials). An external (or internal) magnetic field breaks a Cooper pair by flipping one spin of the Cooper pair. This process is known as "pair breaking". For this reason, the coexistence of superconductivity and magnetic long-range order within a single (thermodynamic) phase seemed to be impossible. Nevertheless, the discovery of superconductivity in the rare-earth (RE), Chevrel-phase compounds $REMo_6X_8$ (X=S or Se) and the XRh_4B_4 (X=Y, Th, or RE) type compounds (1975-1977) [6, 7] has allowed the interplay between superconductivity and magnetism to be studied more easily. In some of these superconductors with long-range ferromagnetic order, there may be a tendency for a physical separation between the superconducting electrons and the magnetic electrons. For example, in $RERh_4B_4$, the electron bands that give rise to superconductivity are believed to be composed primary of 4d-Rh electrons, while the magnetic electron bands are composed primary of 4f-RE

electrons. The physical separation of the superconducting and magnetic electrons may give rise to negligible exchange interaction between the conduction electron spin and the spin of the localized atom (magnetic impurity). Then, only the relatively weak dipole interaction remains to break Cooper pair [6, 7].

Some of the crystals, for example $ErMo_6S_8$ and $SmRh_4B_4$, experience the coexistence of superconductivity and long-range antiferromagnetic order. In this case, the magnetic ordering produces no microscopic magnetic field and, on the order of the scale of the superconducting coherence length, the antiferromagnetic exchange field may average to zero. Thus, the coexistence of superconductivity and antiferromagnetism is not surprising. However, antiferromagnetic order can affect superconductivity by means of a variety of mechanisms, producing anomalies in physical properties in the vicinity of the Neel temperature, the temperature below which the antiferromagnetic order occurs.

For conventional superconductors, magnetic impurities, or an external magnetic field tend to destroy superconductivity. Thus it is believed that in high T_c materials with magnetic order, the superconducting and magnetic phases form spatially separate phases. On the other hand, it can be argued that the close proximity of magnetic and superconductive states may indicate a common origin, or at least a closely related origin. This question still remains unanswered.

The possible clue to this question can be the symmetry of the order parameter, because it is related to the spin of Cooper pair. The possibility of p-wave and spin triplet Cooper pairing on the basis of similarities to ^3He was proposed in [8] for high T_c superconductors with ferromagnetic order. By contrast, for high T_c superconductors with

an antiferromagnetic ordering, spin-singlet pairing in an orbital d-wave channel was proposed in [9]. Recently, many experiments have been done to answer the question about the pair symmetry for many of the high T_c compounds. Although early experiments with high T_c seemed consistent with an s-wave pairing, recent measurements suggest that the pairing state is at least not isotropic. Comprehensive reviews on this topic are given in [8-11]. There are theoretical works suggesting that for some high T_c superconductors with long-range magnetic ordering, a mixture of both p- and d-wave pairing may exist simultaneously [12].

3. Rutheno-Cuprates

The coexistence of high-T_c superconductivity and magnetism was discovered for a rutheno-cuprate of Ru-1222 type, i.e $RuSr_2(R_{1+x}Ce_{1-x})Cu_2O_{10-\delta}$ (where R=Eu, Gd). First reported in 1995 [13, 14] they appear today to provide the first example of superconductivity developing at temperatures far below the transition into a weak ferromagnetic state, with coexistence of both ordering phenomena [15-18].

To properly understand the mechanism that brings about the superconducting state in a particular material it is necessary to know the structures of the compounds that exhibit this phenomenon. All high temperature oxide superconductors are derived from a perovskite prototype structure [19]. A perovskite, in its “ideal” form, is a cubic structure with a relatively large metallic atom (A) at its center, smaller metallic atoms (B) at its corners, and nonmetallic atoms (X) on midpoints between the corners [1]. The “ideal”

perovskite is shown in Figure1. The bulk crystal typically is cubic. The ideal perovskite structure is an insulator because all of the atomic sites are filled and as a result strong ionic bonds hold the electrons firmly in their positions. Since the ideal structure is symmetric, that means it has three-dimensional isotropy.

The superconducting perovskite-like structure differs from the ideal perovskite structure. One of the most significant results is that the material is not isotropic. The structure of the rutheno-cuprates is closely related with that of the "123- cuprates" of the $YBa_2Cu_3O_{7-\delta}$ type [20]. It was shown in [19] that substitutions for Cu in $YBa_2Cu_3O_{7-\delta}$ type compounds have a destructive effect on superconductivity. This supports the belief that the supercurrent flows primarily (if not entirely) in the copper-oxide planes that are perpendicular to the long axis of the crystal structure. That means that supercurrent does not flow, as readily along the long axis, that is perpendicular to the Cu-O planes. In addition, in ordinary or low-temperature superconductors the presence of magnetic impurity ions destroys the superconductivity quite strongly, while in the YBaCuO cases the destruction is selective, depending on how close the substitutions are to the Cu-O layers [21, 22].

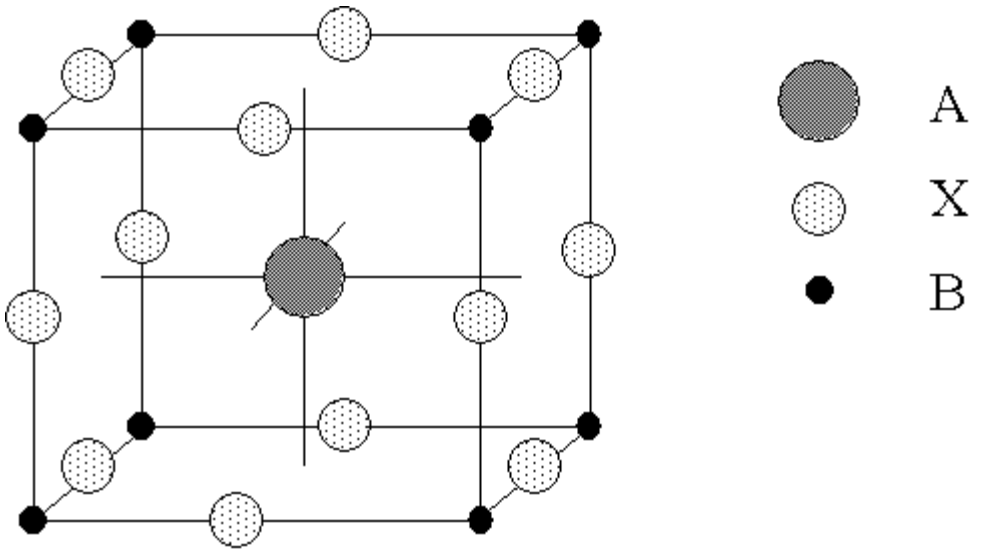

Figure 1. The ideal perovskite (the basic formula is ABX_3).

The structure of the Ru-1222 compound is tetragonal (space group I4/mmm). It evolves from the $RBa_2Cu_3O_7$ structure (where R is the rare-earth) by inserting a fluorite type $(R,Ce)_2O_2$ layer (usually R=Gd or Eu) instead of the R layer in $RBa_2Cu_3O_7$, thus shifting alternate perovskite blocks by (a+b)/2 (see Figure 2) [23, 24].

The oxygen deficiency is a critical factor in determining the superconducting properties in "123-cuprates". This deficiency is associated with the bonding configurations and valence states of the Cu ions that are present. Small losses of oxygen can appreciably change the nearby copper coordination, which at stoichiometry, consists of four, five, or six nearest neighbor Cu-O bonds. Removing oxygen decreases this number of adjacent bonds.

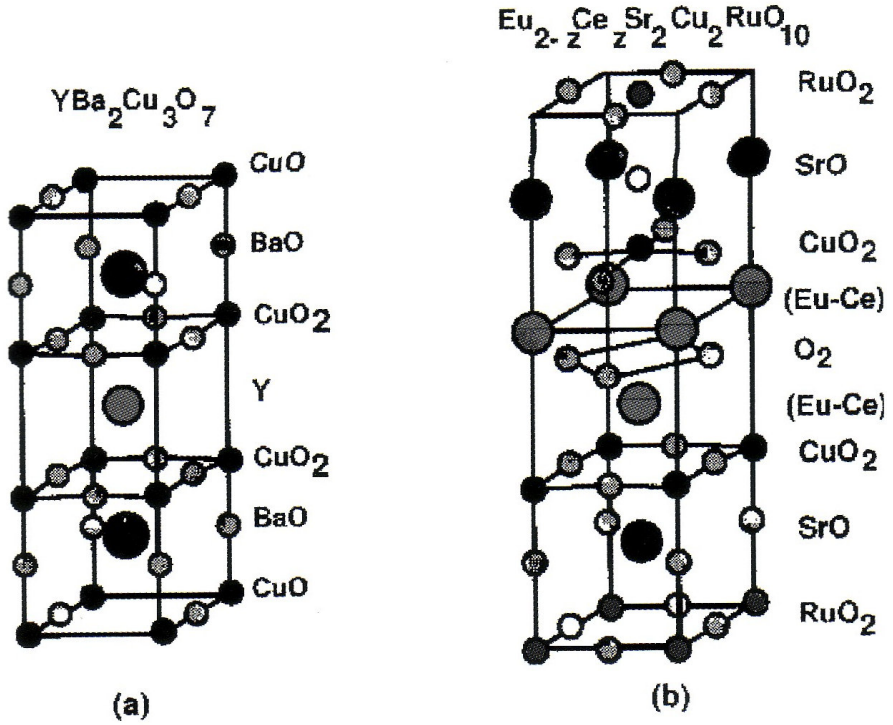

Figure 2. The crystal structure of $YBa_2Cu_3O_7$ and $RuSr_2(Eu_{1-x}Ce_x)Cu_2O_{10-\delta}$.

In the Ru-1222 system with general composition of $RuSr_2(R_{1+x}Ce_{1-x})Cu_2O_{10-\delta}$ (R=Gd or Eu) the Cu oxidation state is adjustable by varying two parameters, the oxygen content and the ratio R : Ce. These parameters appear to be correlated [24]. Nevertheless, it is appropriate to discuss separately the consequences of their variation. The effect of the variation of x on the resistivity behavior is that the superconductivity occurs for Ce contents of 0.4-0.8, with the highest T_c obtained for Ce=0.6 [23]. The data

from Bauernfeind [24] suggests that the highest T_c was achieved in the sample with the highest oxygen content.

The simultaneous occurrence of superconductivity and unusual magnetism in R-1222 compounds was first shown by Bauernfeind, et. al. [14]. Coexistence of weak-ferromagnetic order and superconductivity in Ru-1222 on a microscopic scale was reported by Felner et. al. [15]. According to [16], Ru-1222 materials exhibit coexistence of bulk superconductivity (T_c=32, 42 K) in the magnetic state (T_M=125, 180K) for R=Gd and Eu, respectively. The critical temperatures depend on oxygen concentration and sample preparation. Here T_M/T_c ~ 4, a trend which is contrary to that observed in intermetallic systems. The superconducting charge carriers originate from the CuO_2 planes, and the weak-ferromagnetic state is confined to the Ru layers. Superconductivity survives because the Ru moments probably align in the basal planes, which are practically decoupled from the CuO_2 planes, so that there is little pair breaking.

The close proximity of ferromagnetic and superconductive states in high T_c superconductors may lead to the idea that the electron-electron attraction required to form Cooper pairs might arise, not from phonons, but from some kind of ferromagnetic magnons (magnon-mediated pairing), and those ideas are being studied [6]

B. Samples

Thermal conductivity, thermopower, and electrical resistivity were measured for $(Gd_{1.5}Ce_{0.5})RuSr_2CuO_{10-\delta}$ samples both as prepared by the solid-state reaction method [16, 25] and annealed (12 hours at 845^o C in pure oxygen at 30, 62, 78 atm) samples

were measured. The same type of measurements were made on both samples as prepared and annealed (24 hours at 800^{o} C in pure oxygen at 100, 50 atm) of $(Eu_{1.5}Ce_{0.5})RuSr_2CuO_{10-\delta}$. All of the samples are pressed powder samples and provided by I. Felner and his research group at Hebrew University of Jerusalem.

C. Measurements

1. Thermal Conductivity

The thermal conductivity of all of the samples has been measured by using the steady-state linear heat flow method. The measurements have been performed over the temperature range from 2K to 300K.

If the amount of heat flowing into a body is exactly equal to the heat flowing out, then the temperature will be different at different points within the body but for any given point the temperature will remain constant as a function of time. This condition is called the steady-state and refers only to those cases where the temperature at any given point within a body is independent of the time [26]. Linear flow of heat through the sample (longitudinal heat-flow method) has been achieved by holding the specimen between a heater and a heat sink.

In the steady-state experimental arrangement, illustrated schematically in Figure3, heat is supplied at one end of the rod of uniform cross-sectional area A at a known rate $\dot{Q}$ and is removed at other end. Thermometers are attached at two places

along the specimen separated by distance L, and the temperature difference ΔT between them is measured. The conductivity is then derived from the relation (1):

$$k(T) = \frac{\dot{Q}}{A}\frac{L}{\Delta T} \qquad (1)$$

where $\Delta T = T_2 - T_1$ and $\dot{Q}$ dot is heat flow.

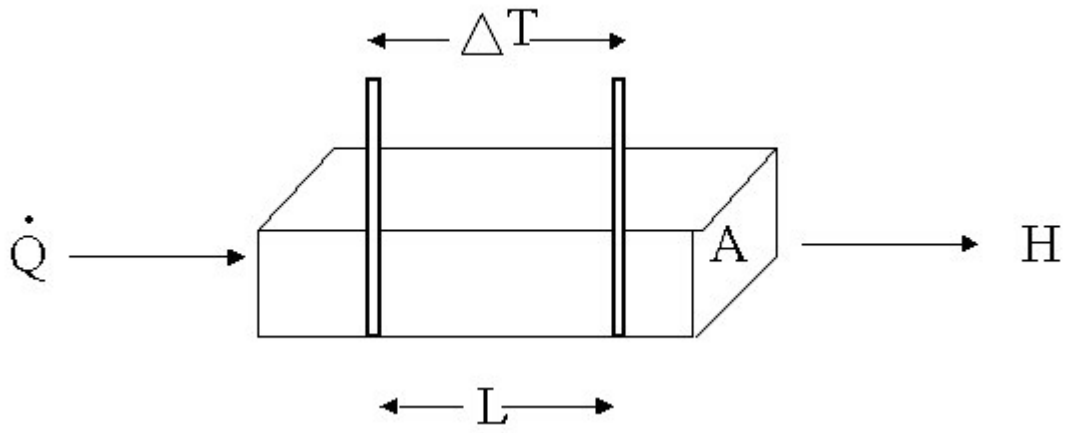

Figure 3. The steady-state longitudinal heat flow method for measuring thermal conductivity.

If ΔT is not too large, the derived value for κ will be the one that corresponds to the mean temperature between the thermometers [27, 28]. In the present experiment the temperature difference was no greater then 5% of the base temperature below 4K, no greater than 3 to 4% of the base temperature above 4K, no greater than 2 to 3% of the

base temperature above 30K, and no more than 1-1.5% above 100K. Equation (1) also assumes that the temperature is uniform across the sample, which means that nearly all the heat supplied by the heater actually travels through the specimen to the colder end. In order to minimize the heat exchange through the surrounding medium and along electrical leads, the sample was held in a $1x10^{-6}$ Torr or better vacuum, and leads to measure the temperature gradient and voltage across the sample were 0.001 inch diameter wires. In order to minimize heat exchange by radiation, a radiation shield, along which there is the same temperature distribution as exists along the sample was used.

In non-magnetic solids, heat is carried both by charge carriers (electrons or holes) and by phonons (quantized lattice vibrations). The total thermal conductivity consists of the sum of these two contributions:

$$\kappa = \kappa_e + \kappa_{ph} \qquad (2)$$

where "e" and "ph" denote the electrons and phonons, respectively.

To a first approximation, κ_e is inversely proportional to the electrical resistivity ρ_e. For pure metals, which have a low value for ρ_e, the contribution due to electrons is much larger than the contribution due to phonons. In contrast, for alloys, which are of substantially larger ρ_e, the contribution due to phonons is no longer negligible [29].

In a magnetic state, in addition to contributions due to charge carriers and phonons, the magnetic ions can also participate in the heat conduction process. In

ordered magnetic crystals the spin system (magnons) can conduct heat and increase the thermal conductivity and at the same time can act as a source of phonon scattering (decrease thermal conductivity) [27]. In the paramagnetic state scattering off of randomly oriented magnetic moments (magnetic disorder scattering) can appreciably reduce the thermal and electrical conductivity of the electrons.

When a material is in the superconducting state, it is in a highly ordered state, where superconducting electrons cannot carry entropy. That means that Cooper pairs cannot carry thermal energy nor can they scatter phonons. With decreasing temperature the number of Cooper pairs increases, and the contribution of the "normal" electrons correspondingly decreases, which will result in a rapid decrease of the electronic heat conduction. At the same time the conduction by phonons will be enhanced, as they are no longer scattered as much by electrons [30].

In summary, the thermal conductivity measurements can be helpful in determining the fraction of the thermal energy that is transported by charge carriers and the amount carried by the phonons. It can also provide information about the interaction between heat carriers: electron-phonon or phonon-magnon interactions. Hence thermal conductivity is a useful tool in investigating the nature of the superconducting and magnetic states of magnetic superconductors.

2. Thermo-Electric Power

The thermo-electric power of all of the samples has been measured using a steady-state linear heat flow method.

When a temperature gradient is maintained across a conductor or semiconductor sample and no electric current is allowed to flow, there will be a steady-state electrostatic potential difference between the high and low-temperature regions of the specimen. This phenomenon is called the thermoelectric, thermopower, or Seebeck effect. The coefficient which is defined as the potential difference developed per unit temperature difference is called the thermopower S (Seebeck coefficient), i.e.

$$S = \frac{dV}{dT} \tag{3}$$

By convention, the sign of S represents the potential of the cold side with respect to the hot side. If electrons diffuse from hot to cold, then the cold side is negative with respect to the hot side and Seebeck coefficient is negative. In a p-type semiconductor, on the other hand, holes would diffuse from the hot to the cold end. The cold side would be positive with respect to the hot side which would make S a positive quantity. Thus the sign of the thermopower determines whether the carriers in the given specimen are electrons or holes [31]. However there are deviations from this rule. Thermopower can be very sensitive to phonon-electron scattering (phonon drag). According to Barnard [32], the interaction of an electron with the lattice which produces resistance is described as an electron-phonon interaction and results in either the creation or annihilation of a phonon. In the former case momentum and energy are transferred from the electron system to the lattice and in the latter they are communicated to the electron system. Thus

the temperature gradient in a crystal results in the creation of a phonon flux which can interact with other phonons, impurities and electrons. The contribution from phonon-drag is most important in the temperature region where phonon-electron scattering is predominant. According to MacDonald [33] this happens for temperatures from $0.1\theta_D$ to $0.3\theta_D$, where θ_D is the Debye temperature. Examples of flipping the sign of thermopower for some semiconductors at low temperatures due to phonon-electron scattering processes are discussed in [34].

A sample that is in the superconducting state cannot sustain any potential difference caused by the temperature gradient. Hence the Seebeck coefficient in the superconducting state is equal to zero. The absence of a potential difference across a superconductor in the presence of the temperature difference across its ends can be explained by the fact that superconducting electrons will screen any electric field inside the superconductor in the static state. Thus measurements of thermo-electric power indicate the transition to the superconducting state, but at the same time they do not provide any information about the superconducting state itself.

3. Electrical Resistivity

The electrical resistivity of all samples versus the temperature has been measured by using the standard four-terminal method. The measurements have been performed from 4K to 300K. The four-terminal measurement method eliminates the effect of lead resistance. Four-terminal measurements are done by applying a current and measuring

voltage. Figure 4 shows a typical configuration for a four-terminal measurement, the constant current power supply is used to force a current through the sample. The digital multimeter measures the resulting voltage drop across the sample.

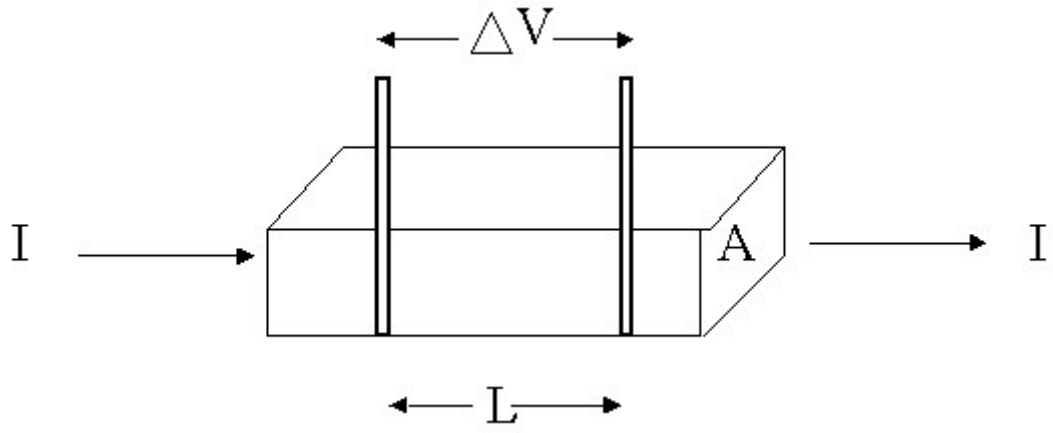

Figure 4. The standard four-probe resistance measurement approach.

If measurements are done at low temperatures, thermal EMF's may contribute to errors in this type of measurement. Thermal EMF is the physical phenomenon when a thermal voltage is induced across the wire because its two ends may be at different temperatures. To eliminate thermal EMF, the DC source current direction was changed by using polarity reversal. The resistance of the sample was measured using both positive and negative currents of the same magnitude. In this case the two resistivity values are averaged so that the offsets caused by thermal EMF cancel each other [35].

In a metal, the free electrons responsible for electrical conduction are scattered by imperfections in the crystal lattice and by the thermal vibrations of the lattice. These

processes limit the conductivity and so determine the electrical resistivity. Matthiessen's rule states that the total resistivity can be written as the sum of two components: the resistivity due to the static imperfections either chemical or physical impurities- and a resistivity caused by thermal vibrations [36]. Due to the static character of the impurities, the resistivity due to the phonon scattering is the quantity that changes with temperature.

This rule is applicable when electrons can be considered as free particles without strong many-body effects. When a material is in magnetic state, electrons can also scatter on randomly oriented magnetic moments. As a result, the resistance decreases rather abruptly on a transition to a magnetically ordered state.

The electrical resistivity data are a useful tool in investigation of superconductors. First, from resistivity data the superconducting transition temperature can be obtained. Second, the width of the transition to the superconducting state gives information about the quality of the sample. A sharp transition indicates a high purity sample. A very broad transition indicates a granular sample in which the transition to superconducting state does not appear simultaneously in all granules. Finally, the resistivity data together with thermal conductivity data can be used together with the Wiedemann-Franz Law to estimate the fraction of thermal conductivity that is due to the charge carriers. The remaining part will be the thermal conductivity due to phonons.

II EXPERIMENT

A. Thermo-Electric Power and Thermal Conductivity Measurements

Thermal conductance and thermo-electric power were measured simultaneously with the same temperature gradient across the sample. The resistance measurements were taken separately with the sample at uniform temperature using the standard four-probe resistance approach.

1. Measurement Setup

The block diagram of the setup for thermopower and thermal conductivity measurements is shown in Figure 5. The setup consists of three main parts: the system (cryostat), external circuitry, and CPU with data acquisition interface.

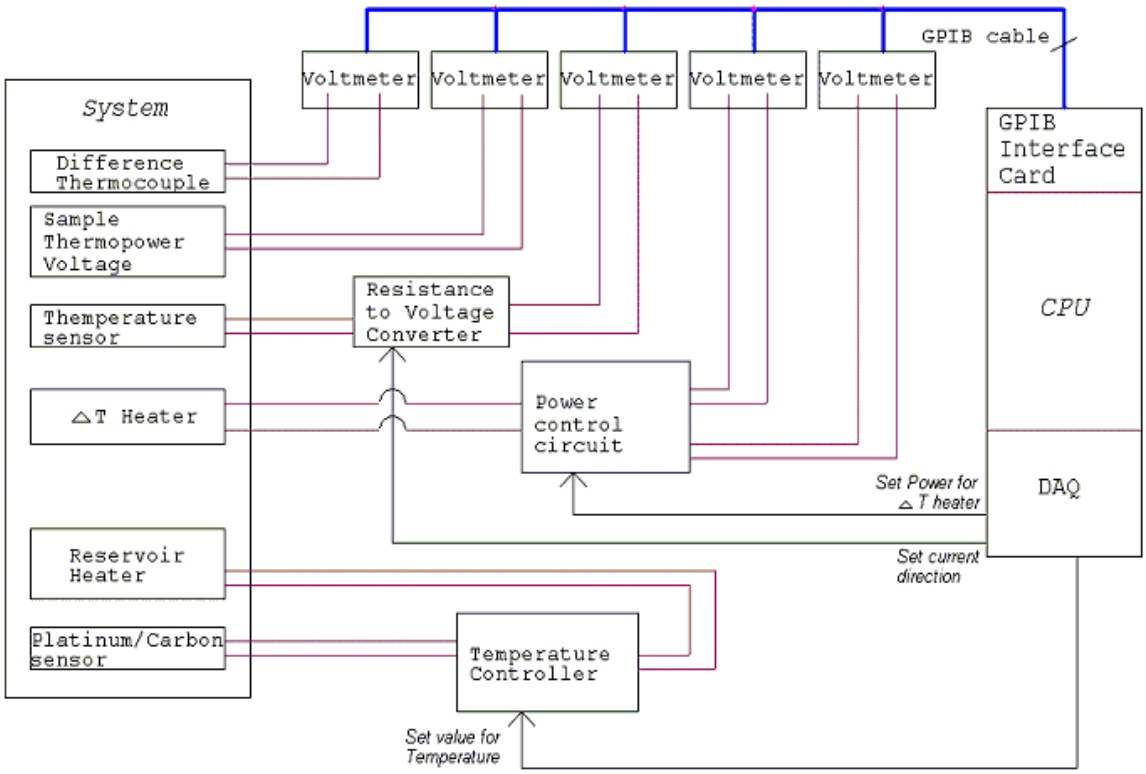

Figure 5. The block diagram of the setup for measurements of thermal properties.

a) System

The system is the cryostat that consists of the sample, two heaters (one to establish delta T across the sample and one to control the temperature of the cold end of the sample, i.e. the temperature reservoir), and sensors for temperature measurements and control. The detailed description of the cryostat is in Subsection C below.

b) Sensors

Thermocouple. Gold-0.07 atomic percent iron with Chromel (Au0.07%Fe-Cr) thermocouple was used to measure the temperature gradient across the sample for thermal power and thermal conductivity measurements. The thermocouple is directly attached to the sample (but electrically insulated from it) in the way described in Subsection D below. Two 0.001 inch Chromel leads of the thermocouple are thermally connected to the thermal reservoir (but electrically insulated from it) where they are electrically attached to two 0.003 inch Chromel wires. The two 0.003 inch Chromel wires are thermally anchored to the thermal reservoir and go directly to a digital nanovoltmeter at room temperature. This arrangement minimizes the heat leak to the sample space.

Thermo-electric Power wire. To measure the voltage induced across the sample as a result of the temperature difference across the sample, two 0.001 inch (0.025 millimeters) Manganin wires were used. At one end, they were directly attached to the sample in the way described in Subsection D below. At the other end, they are thermally connected (but electrically insulated) to the thermal reservoir and electrically connected to two 0.004 inch Manganin wires. The two 0.004 inch Manganin wires are thermally anchored to the thermal reservoir and go directly to a digital nanovoltmeter at room temperature.

Temperature sensors (for temperature measurements). Three sensors were used to measure the temperature from 1.7K to 300K during the experiment. A germanium resistance temperature sensor was used to measure temperature from 1.7 to

5K. A Carbon-Glass or Carbon resistance sensor was used to measure temperature from 5K to 40K. A platinum resistance sensor was used for the temperature range from 40K to 300K. The contact wires from the temperature sensors are attached to a resistance-to-voltage converter external circuit.

Temperature sensors (for temperature control). Two sensors were used to control the temperature during the experiment from 1.7 K to 300K. Carbon resistance sensor was used to control the temperature from 1.7 K to 35 K. Platinum resistance sensor was used to control the temperature from 35K to 300K. The leads from those two sensors go to the temperature control external circuitry.

c) Heaters

The Main Heater. The main heater is a coil made of Manganin wire (R=68 Ohm) to heat the copper block, which serves as constant temperature reservoir for the sample. The contact wires from the main heater go to the external temperature controller.

The Δ T Heater. A small heater made from a RuO thick film is attached to the small delta-T block, which in turn is attached directly to one end of the sample as shown in Subsection D below. The Δ T heater is used to generate the temperature difference, Δ T, across the sample.

To avoid a heat leak to the sample space from outside, all of the wires used inside the cryostat which go to the voltmeters at room temperature were thermally anchored to the thermal reservoir.

2. External Circuitry

a) Temperature Measurement

The signal conditioning circuit for temperature measurements with Germanium, Platinum or Carbon-Glass resistance thermometers is shown in Figure 6. This circuit is the Resistance-to-Voltage Converter circuit that converts the resistance to a voltage, which can be processed in the computer that controls the experiment and processes the data.

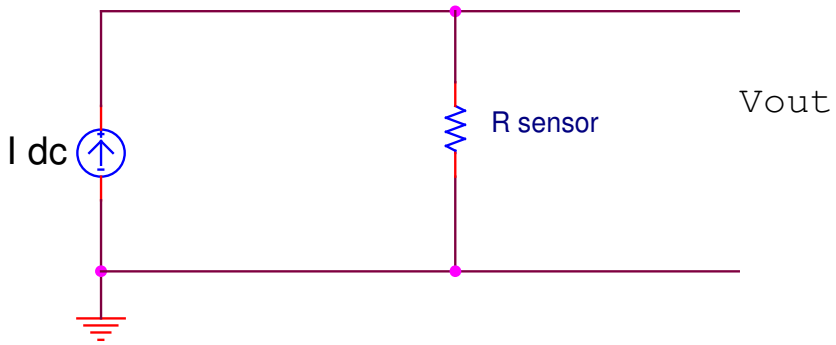

Figure 6. The Resistance-to-Voltage converter circuit for temperature measurement sensors.

The resistance to voltage converter circuit converts the resistance of the temperature sensor to a voltage. This circuit consists of constant current supply and resistive sensor in series. In order to convert the resistance of the sensor to the corresponding voltage, the specified current is passed through the sensor, and the output voltage is measured with a digital multimeter. Depending on the temperature of the surrounding environment, three different values of the current were used: I=1uA from

1.7 K to 5 K, I=10uA from 5 K to 40 K, and I=100uA from 40K to 300 K. The given values for current were chosen: first, to provide safe operation of the temperature sensors, which can be destroyed by high current values and, second, to prevent self-heating of the temperature sensors that can lead to the temperature of the thermometer being hotter than the surrounding temperature and thus introduce an error in the temperature readings, especially at low temperatures. By knowing the current through the sensor and measuring the corresponding voltage across the sensor, the voltage is converted back to a resistance in the CPU and compared to the R versus T calibration table for the particular thermometer.

b) Temperature Control

The temperature control is a closed-loop system. The block diagram for the temperature control system is shown in Figure 7. The more detailed techniques of temperature control circuits are described by W.Bolton in his book [37]. The input to the heating process depends on the error signal that is the output from the comparison element. The purpose of the comparison element is to determine the difference between the required temperature initially set and the actual temperature fed back from the output of the system. The error signal controls the process. If there is a difference between the signals then the actual output is not the same as the desired output. When the actual output is the same as the required output then there is zero error.

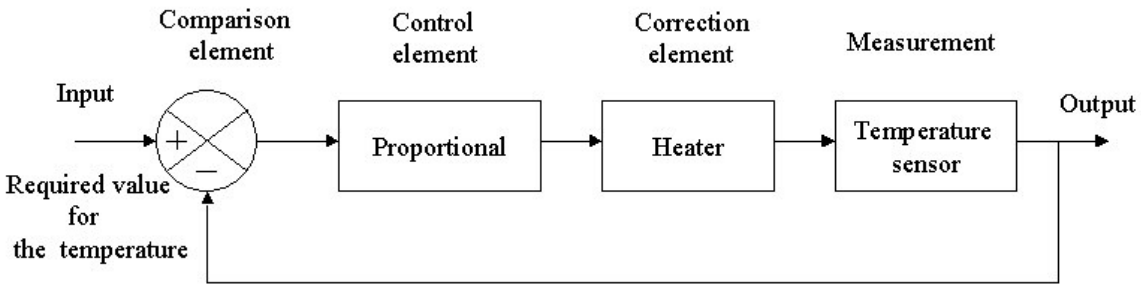

Figure 7. The block diagram for temperature control circuit.

The control law element determines what action to take when an error signal is received. In our experiment, the signal produced by control law element is proportional to the size of error. The correction element produces a change in the process, which aims to correct or change the controlled condition. In our temperature control system, the correction element is a heater, which is used to reach the required temperature. The measurement element produces a signal related to the variable condition of the process that is being controlled. In the present experiment the measurement element is the temperature sensor. At low temperatures, between 1.7 K and 40 K, a Carbon sensor was used. At high temperatures, between 40K to 300 K, a Platinum resistor was used.

The circuit for the temperature controller is shown in Figure 8. The resistance to voltage converter circuit is a Wheatstone bridge. The resistive temperature sensor forms one of the arms of the bridge. The lower part of the arm of the bridge consists of a potentiometer and stepper motor in series. They are used to set manually or with the CPU the initial input value to the temperature control system. The second arm of the

bridge consists of a potentiometer that is used to control the sensitivity of the bridge. The output from the bridge is fed to the comparison element. The comparison element is a differential amplifier with variable gain. The output from the amplifier goes to the band-pass filter that is used to eliminate the frequencies different from the frequency of the power supply used to power the bridge in the temperature control circuit. After the filtering, the error signal goes to the control element, which is a voltage to current converter with final amplification stage. The voltage to current converter produces a current proportional to the voltage of the error signal. In our experiment, a lock-in-amplifier was used to power the resistance bridge, the comparison element and filter.

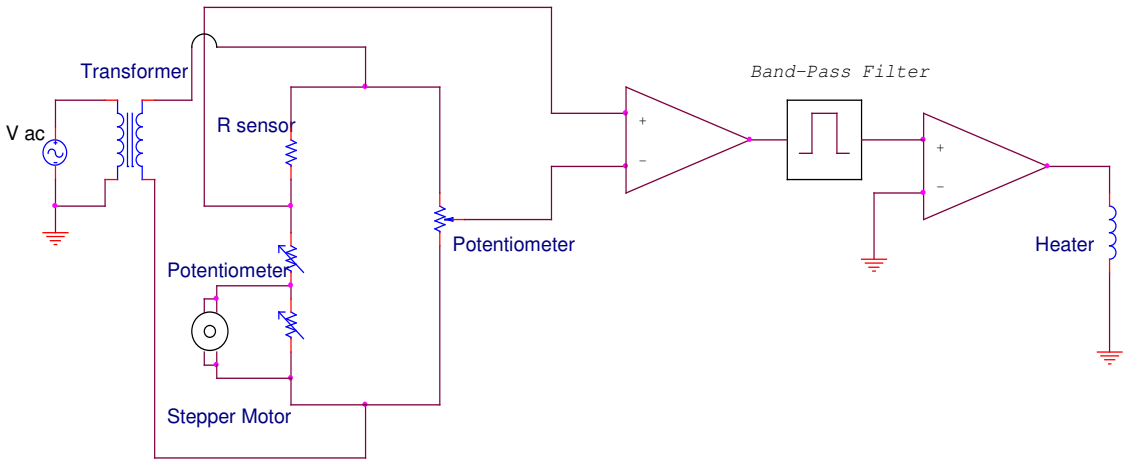

Figure 8. The circuit for the temperature control in the system.

c) The Δ T heater Power Control Circuit

The Power Control Circuit is used to control the amount of heat through the sample for the thermoelectric power and thermal conductivity measurements. Four wires go from the small heater to the power control circuit: two wires are for current and two wires are for voltage measurements.

As we pass the current through the small heater (RuO thick film), heat is generated. Since the experiment is carried out at high vacuum about $1*10^{-6}$ Torr or better, the amount of heat generated in the small heater is assumed to pass through the sample without loss. That means that by measuring the power released from the small heater, we know how much heat passes through the sample, i.e. we know $\dot{Q}$ in the formula (1).

The power control circuit is shown in Figure 9.

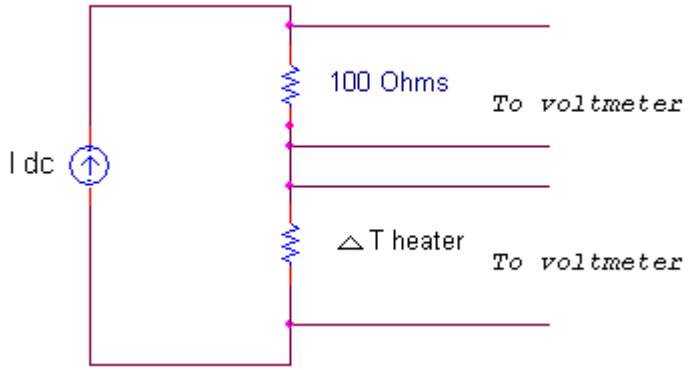

Figure 9. The circuit to control power in the Δ T heater.

The circuit consists of current power supply and a 100 Ohm standard resistor in series with the Δ T heater. By measuring the voltage across the 100 Ohm resistor, one can find the current through the small heater. Simultaneously, by measuring the voltage across the heater, one can calculate the power generated by the ΔT heater or, equivalently, the amount of heat that passes through the sample. The amount of current through the Δ T heater controls the power generated on it.

d) Data Acquisition

The data acquisition was done with a MacIntosh computer by using LabVIEW 3.1 to configure and control the Instrument Control System and DAQ System.

The Acquisition Interface consists of two parts: the Instrument Control System and a plug-in DAQ (Data Acquisition Board).

The Instrument Control System consists of a General Purpose Interface Bus (GPIB) and GPIB Interface Card. The GPIB cable connects digital multimeters to the CPU via the GPIB Interface card. The purpose of the Instrument Control System is to provide the communication between CPU and external devices (in our case digital multimeters). A digital multimeter converts the analog voltage across the temperature sensor to the corresponding digital value that is transferred by means of the Instrument Control System to the CPU for storage and further processing. The data transfer is controlled by the CPU.

The task of a DAQ system is the measurement or generation of physical signals. During the experiment two functions were used: Analog Output and Digital Output. Analog Output function was used to control the amount of heat generated in the Δ T heater by controlling the current through it in the Power control circuit. Digital Output was used to perform two functions. The first function was to set the required value for temperature by controlling the stepper motor in the Temperature Control circuit. The second function was to change the direction of the current through the temperature sensor in the Resistance-to-Voltage converter circuit to cancel the induced thermal EMF in the leads for more accurate temperature measurement.

B. The Resistance Measurements

1. Measurement Setup

The block diagram of the setup for the resistance measurements is shown in Figure 10.

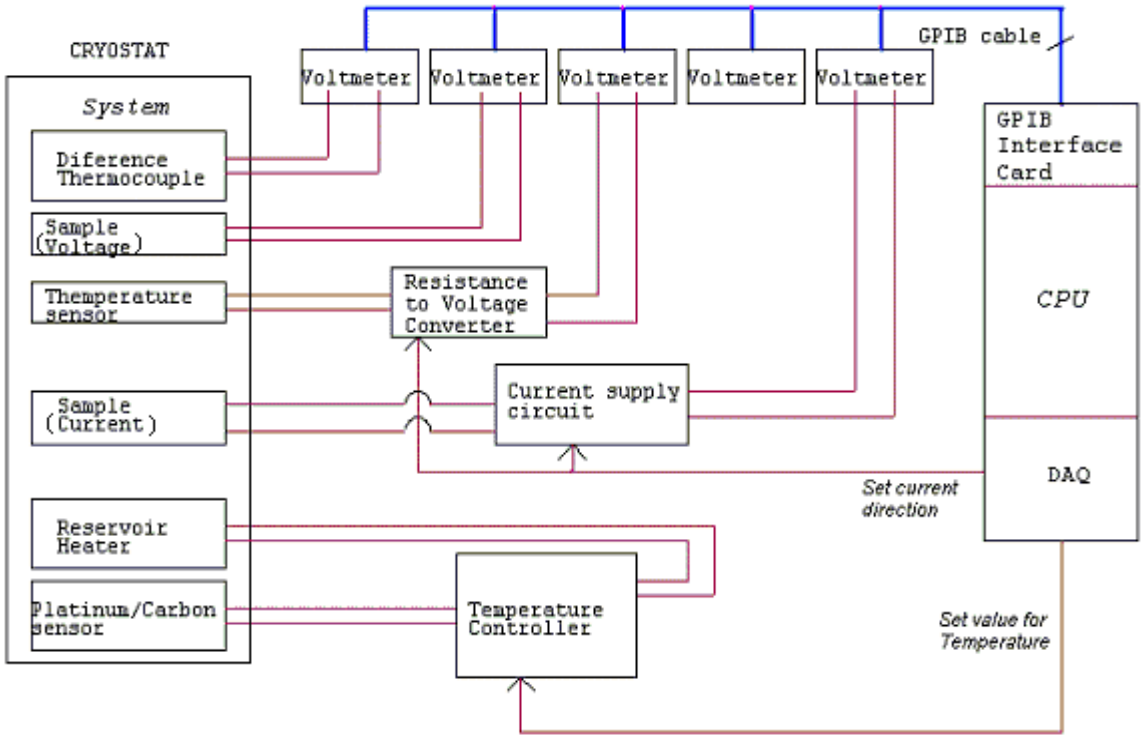

Figure 10. The block diagram of the setup for measurements of resistance.

The setup for resistance measurement consists of three main parts: the system, external circuitry, and CPU with data acquisition interface.

a) System

The system is the cryostat that consists of the sample, one heater (to control the temperature of the sample, i.e. the temperature reservoir), and sensors for temperature measurements and control. The detailed description of the cryostat is in Subsection C below.

Thermocouple. Since the experiment was held in high vacuum during measurement process and the samples being measured have small thermal conductivity, the fast process of taking data over a wide range of temperature may lead to a non-equilibrium state and consequently to a temperature difference across the sample. In order to avoid the error in measurements, the difference thermocouple was used to monitor the temperature difference across the sample.

Sample Voltage Wire. To measure the voltage across the sample as the result of passing current through it, 0.001 inch Manganin voltage leads are used. This is the same wire that was used in the thermo-electric power measurements for measuring the voltage induced across the sample as the result of a temperature difference across it.

Sample Current Wire. 0.003 inch Manganin wire was used to pass the current through the sample. For $RuSr_2(Gd_{1.5}Ce_{0.5})Cu_2O_{10-\delta}$ samples, 1mA was used; for $RuSr_2(Eu_{1.5}Ce_{0.5})Cu_2O_{10-\delta}$ samples, 10mA was used. During the temperature measurement process, the CPU controlled the direction of current through the sample.

Temperature sensors (for temperature measurements). See the subsection for Thermo-Electric Power and Thermal Conductivity measurements.

Temperature sensors (for temperature control). See the subsection for Thermo-Electric Power and Thermal Conductivity measurements.

b) Heaters

Main Heater. This is the only heater that was used to control the temperature of the sample. See the subsection for Thermo-Electric Power and Thermal Conductivity measurements.

To avoid a heat leak to the sample space from outside, all of the wires used inside the cryostat which go to the voltmeters at room temperature were thermally anchored to the thermal reservoir.

2. External Circuitry

The circuits for temperature measurement and temperature control are the same as for the thermal property measurement setup. The only difference is that instead of the Power control circuit, the Current control circuit was used.

a) Current Control Circuit

The schematics for the circuit is shown in Figure 11.

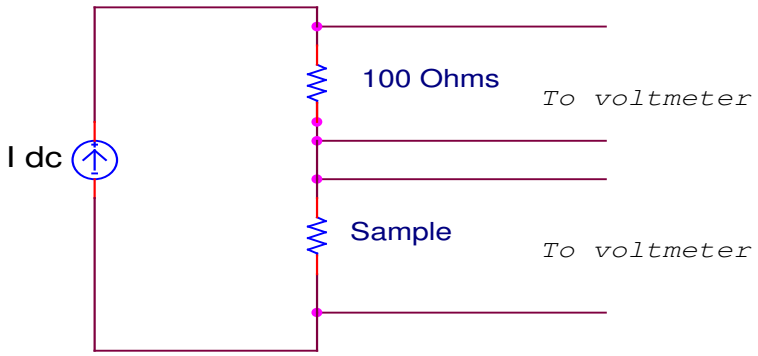

Figure 11. The circuit to control current through the sample.

The circuit consists of the Constant Current Power Supply and the sample with a 100 Ohm standard resistor in series. The voltage across the 100 Ohm resistor was measured with a multimeter. In order to monitor the current through the sample.

b) Data Acquisition

The data acquisition process is the same as for the thermal property measurements. Two digital channels from the DAQ were used to control the direction of current through the sample and the temperature sensors and to set the temperature in the temperature control circuit.

C. Cryostat

The electric and thermal properties were measured in the cryostat constructed in our laboratory. The overall picture of the cryostat is shown in Figure 12. The cryostat contains a stainless steel vacuum can that contains the sample space and a 1-Kelvin pot. The sample space is pumped out during the experiment through the vacuum can pumping line. The 1 K pot is used to achieve a temperature lower than the boiling point of liquid helium temperature, 4.2 K. Around 4.2 K, the 1 K pot is filled with He^4 and is pumped out through the 1 K pot pumping line to achieve the lowest temperature of 1.7 K. To fill the 1 K pot with liquid helium, the 1 K pot Liquid Helium Fill Valve was used. The Liquid Helium Level Detector is used to measure the liquid helium level in the liquid helium bath which surrounds the vacuum can.

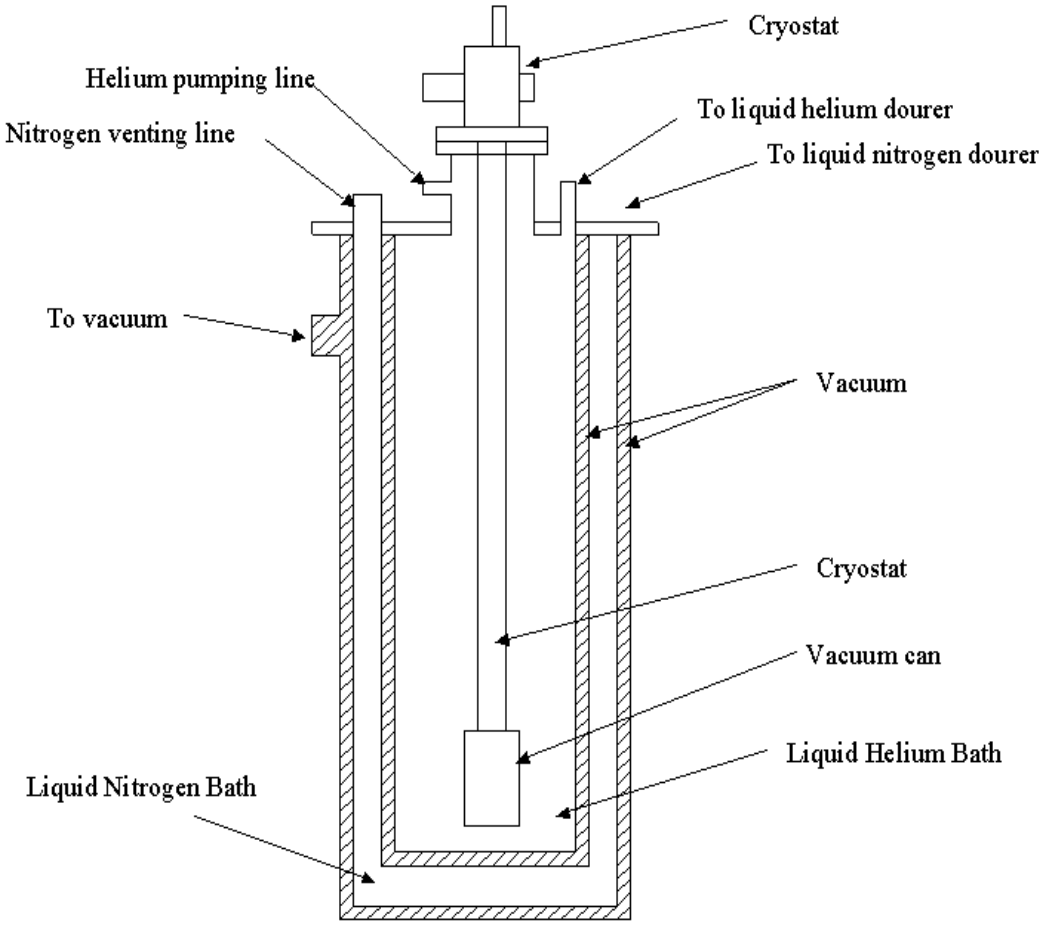

Figure 12. The overall schematic drawing of the system.

Figure 13 shows the cryostat inside the measurement system. To achieve 1.7 K the following procedure was performed. First, the temperature inside the sample space was lowered to 77 K by filling liquid nitrogen into the Liquid Nitrogen Space. Second, as soon as the temperature was around 80 K, liquid helium was transferred to the Liquid

Helium Bath. During the liquid helium transfer, as soon as the temperature was around 60 K, the transfer was stopped and the helium gas was pumped from the sample space. This procedure was done to avoid condensing helium gas inside the sample space. Presence of helium gas in the sample space around 4.2 K will create a large heat leak and, consequently, will prevent reaching 1.7 K and impair control of the temperature. As soon as the vacuum inside the sample space reached $1*10^{-6}$ Torr or better, the liquid helium transfer was resumed. Further lowering of temperature was done by pumping helium from the liquid helium bath through the 1 K pot. As soon as the temperature reached 4.2 K, pumping of the 1 K pot was stopped. After that, the 1 K pot was used in the "one-shot" operation mode to achieve 1.7 K. That is, first it was fully filled with liquid helium and then after the 1 K Pot Liquid Helium Fill Valve had been closed, the 1K pot was pumped to cool the sample to the desired temperature.

Figure 14 shows the internal content of the vacuum can in detail. The vacuum can consists of the sample space and the 1 K pot. The sample space can be divided into two regions: the cold and the hot region. The sample is placed between these two regions. The hot region is the Δ T heater block, which is a ruthenium-oxide thick film heater. The function of the Δ T heater is to supply the flow of heat through the sample for delta-T measurements in the thermal conductance and the thermo-electric power measurements. The block with the Δ T heater is attached to one end of the sample; the second end of the sample is attached to the cold end, which is the sink for the heat from the hot end. The cold region is the copper block that contains three temperature sensors

for the temperature measurements, two temperature sensors for temperature control of the system and the big heater to establish the base temperature.

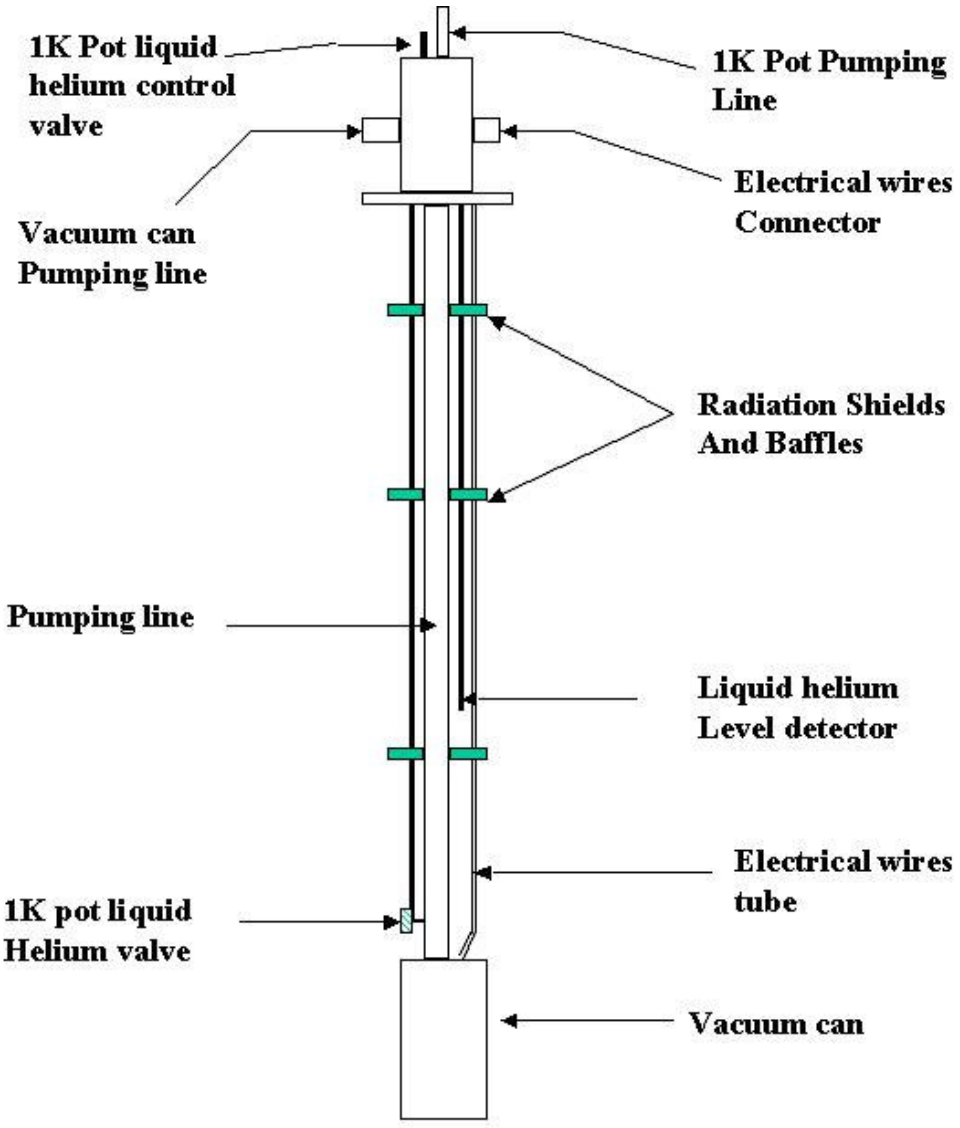

Figure 13. The cryostat.

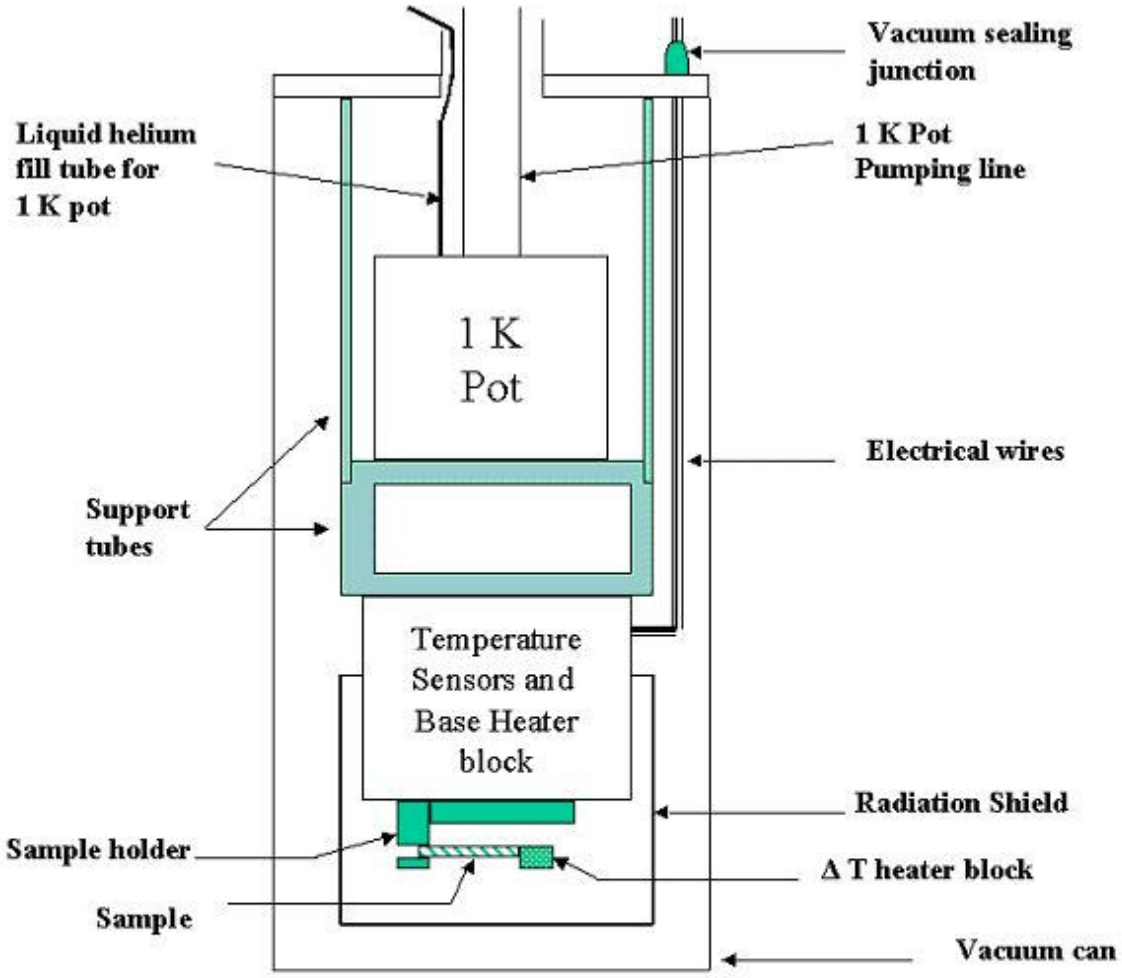

Figure 14. The vacuum can.

D. Sample Mounting

Figure 15 represents the way the sample was mounted in the cryostat. One end of the sample is attached to the Δ T heater block; the other end is attached to the supportive copper piece. If the sample was not large enough to clamp its end to the base part, the copper piece was used to support the sample from the base. The supportive piece and the Δ T heater were attached to the sample using electrically conductive silver epoxy.

The delta T heater block consists of a ruthenium-oxide thick film heater (Mini Systems, Inc.). The ruthenium-oxide thick film is thermally anchored and attached to the delta T block with EPO-TEK 920 thermally conductive epoxy.

To avoid any error in measurements of the temperature difference and the corresponding induced voltage difference across the sample, both a 0.001 inch (0.025 millimeter) Gold-0.07 atomic percent Iron with Chromel thermocouple and a 0.001 inch (0.025 millimeter) Manganin wire sensor (used for thermo-electric Power measurements) were directly attached to the sample with two thin (0.003 inch) short copper rods (about 5 millimeter long). The two copper rods were attached to the sample with silver epoxy.

In case, if the resistance of the contacts with silver epoxy was high, silver paste was used in addition to the silver epoxy to improve the electrical contacts.

To perform the four-contact resistance measurements, the Manganin (0.003 inch) wire, which was used to pass the specified current through the sample, was soldered to the hot end of the sample using a #8 Indalloy (44% indium, 42% tin, 14% cadmium)

solder with a melting temperature of 93 Celsius. To complete the circuit, a second identical wire was soldered to the other end of the sample. The voltage across the sample was measured by using the 0.001-inch Manganing wires that are usually used for thermo-electric Power measurements.

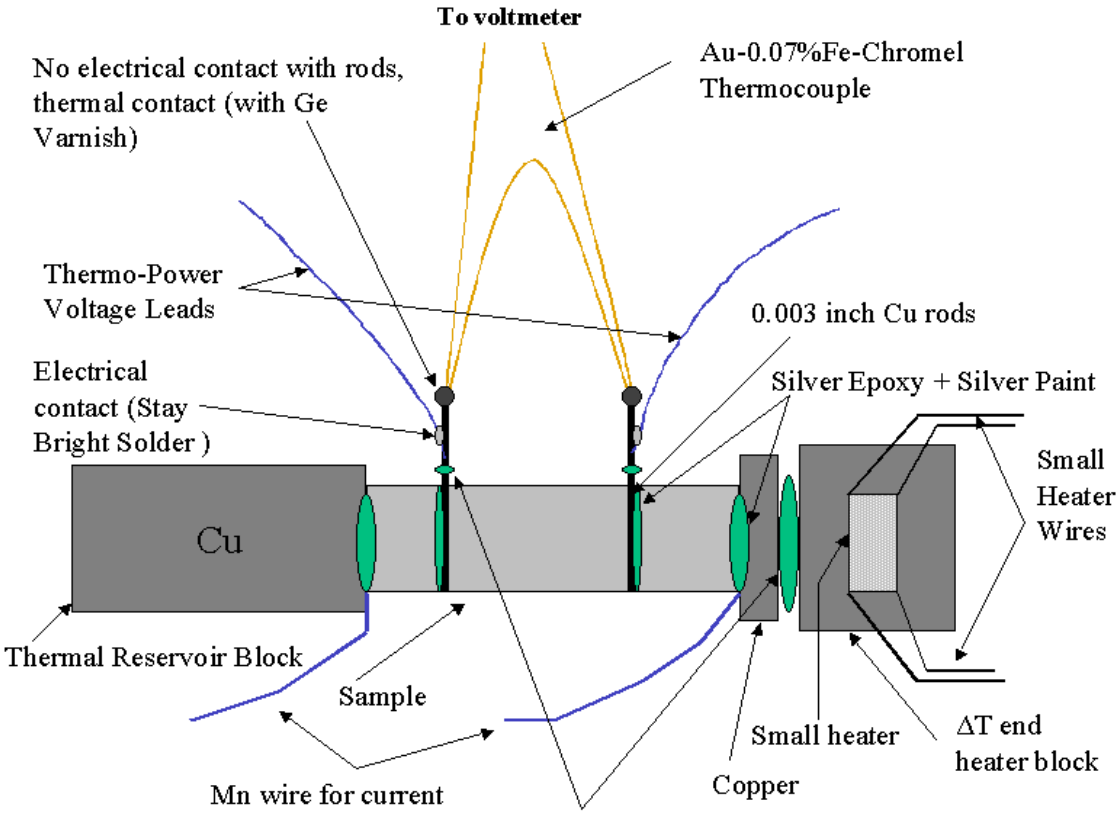

Figure 15. The sample mounting.

III RESULTS

A. Resistivity of $(Eu_{1.5}Ce_{0.5})RuSr_2Cu_2O_{10-\delta}$

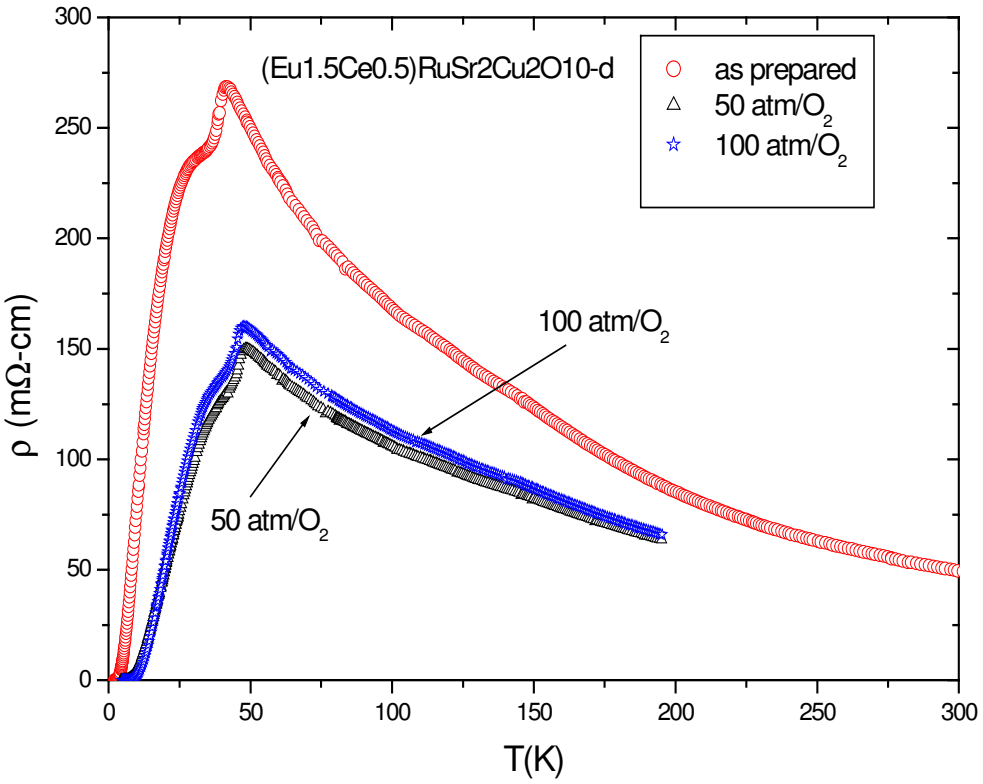

Figure 16. The resistivity ρ of $(Eu_{1.5}Ce_{0.5})RuSr_2Cu_2O_{10-\delta}$ samples with different oxygen content (as-prepared, annealed at 50 atm/O_2 and annealed at 100 atm/O_2) as a function of temperature T.

Figure 16 shows the resistivity versus temperature for $(Eu_{1.5}Ce_{0.5})RuSr_2Cu_2O_{10-\delta}$ (Ru-1222(Eu)) samples with different oxygen content measured from 2K to 300K. All samples show a semiconductor like behavior of the resistivity with decreasing temperature. The as-prepared sample has a steeper increase in resistivity and the highest magnitude comparing to samples annealed in oxygen. All three samples have

superconducting transitions that are rather broad (around 40K) in temperature and have shouldered (or two-stage) features.

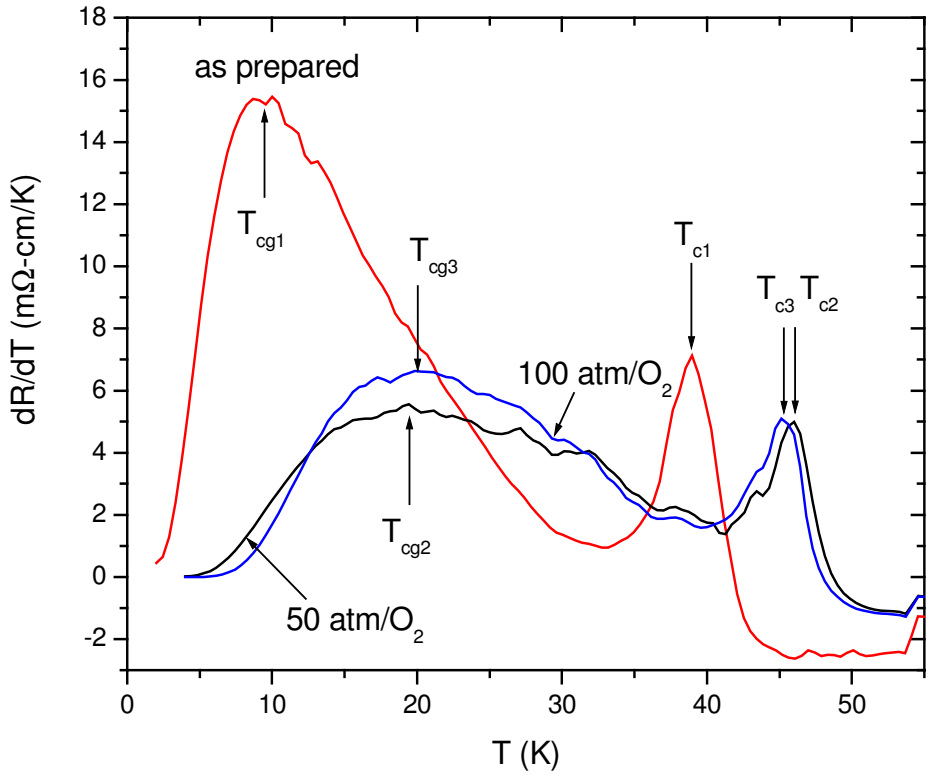

Figure 17. Derivatives versus temperature for $(Eu_{1.5}Ce_{0.5})RuSr_2Cu_2O_{10-\delta}$ sample with different oxygen content (as-prepared, annealed at 50 atm/O_2 and annealed at 100atm/O_2 samples).

Figure 17 shows the derivatives dR(T)/dT versus temperature for Ru-1222(Eu) samples. The derivative curve for each sample reveals two peaks. These two peaks are marked as T_c and T_{cg} in Figure 17.

The ρ(T) and dR/dT curves for the as-prepared sample (which is the most depleted in oxygen) indicate that the onset of superconductivity is at ~39K and T_{c1} and T_{cg1} are equal to 39K and 10K, respectively. The resistivity goes to 0 at T≈3 K. The resistivity data for the sample annealed in oxygen at 50 atm show that T^{onset}≈45K and T_{c2} and T_{cg2} are equal to 45K and 20K, respectively. The resistivity goes to 0 at T≈6.5 K. The sample annealed in oxygen at 100 atm shows very similar behavior to the sample annealed at 50 atm that is T^{onset}≈44.5K and T_{c3} and T_{cg3} are equal to 44.5K and 21.5K, respectively, and the resistivity goes to 0 at T≈8 K. The complete data for T^{onset}, T_c and T_{cg} for all three samples are in the table in Section IV, Subsection A. The ρ(T) data are quite different to those reported in [38, 39]. The difference is in magnitude of the normal state resistivity. It is known that the physical properties of the ruthenocuprates depend on the preparation conditions [40, 41]. This fact does not give much possibility to compare our data with that of the data of the others groups on different Ru-1222 systems.

Thus, the resistivity data show that the process of annealing in oxygen results in a decrease in the normal state resistivity, in an increase of the superconducting transition temperatures T_c and T_{cg}, and suppression of the shoulder feature at T_{cg}. Comparing samples annealed in oxygen, it can be noted that T_c and T_{cg} are closer for the sample annealed at 100 atm/O_2.

B. Thermopower of $(Eu_{1.5}Ce_{0.5})RuSr_2Cu_2O_{10-\delta}$

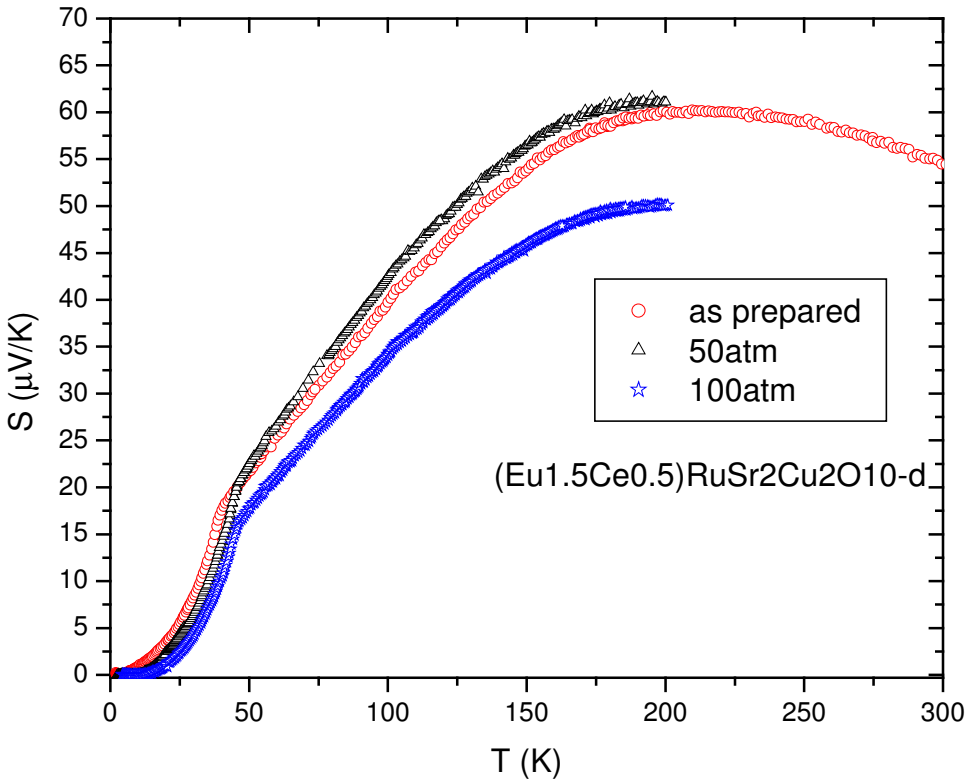

Figure 18. The thermopower versus temperature for $(Eu_{1.5}Ce_{0.5})RuSr_2Cu_2O_{10-\delta}$ sample with different oxygen content (as prepared, annealed at 50 atm/O_2 and annealed at 100 atm/O_2).

Figure 18 shows the absolute thermopower for the as-prepared sample of Ru-1222(Eu) measured from 1.8K to 300K and for samples annealed in oxygen measured from 1.8K to 200K. All samples show a rather large magnitude for the absolute thermopower. The as-prepared and the sample annealed at 50 atm have very close values for thermopower above the superconducting transition. S(T) for the sample

annealed at 100 atm is 16% less at 200K than that for the as-prepared sample and the one at 50 atm. The data for S(T) are similar in temperature dependence to that reported earlier [42] and more recently [39].

The thermoelectric power is positive for the entire temperature range, which is consistent with hole charge carriers [39, 42]. The room temperature value of S, i.e. S^{300K}, for the as-prepared sample is found to be around 55 μV/K. All three curves pass through a maximum (TEP maximum) at around 220K. The annealing in oxygen seems to shift the TEP maximum to lower temperatures. The S(T) data for all three samples show a sharp break in the slope of S(T) at T=39K and T≈45K for the as-prepared sample and the samples annealed in oxygen, respectively, which corresponds to the superconducting transition temperature T_c and agrees with T_c or T^{onset} determined from the resistivity data shown in Figure 17.

C. Thermal Conductivity Data for $(Eu_{1.5}Ce_{0.5})RuSr_2Cu_2O_{10-\delta}$

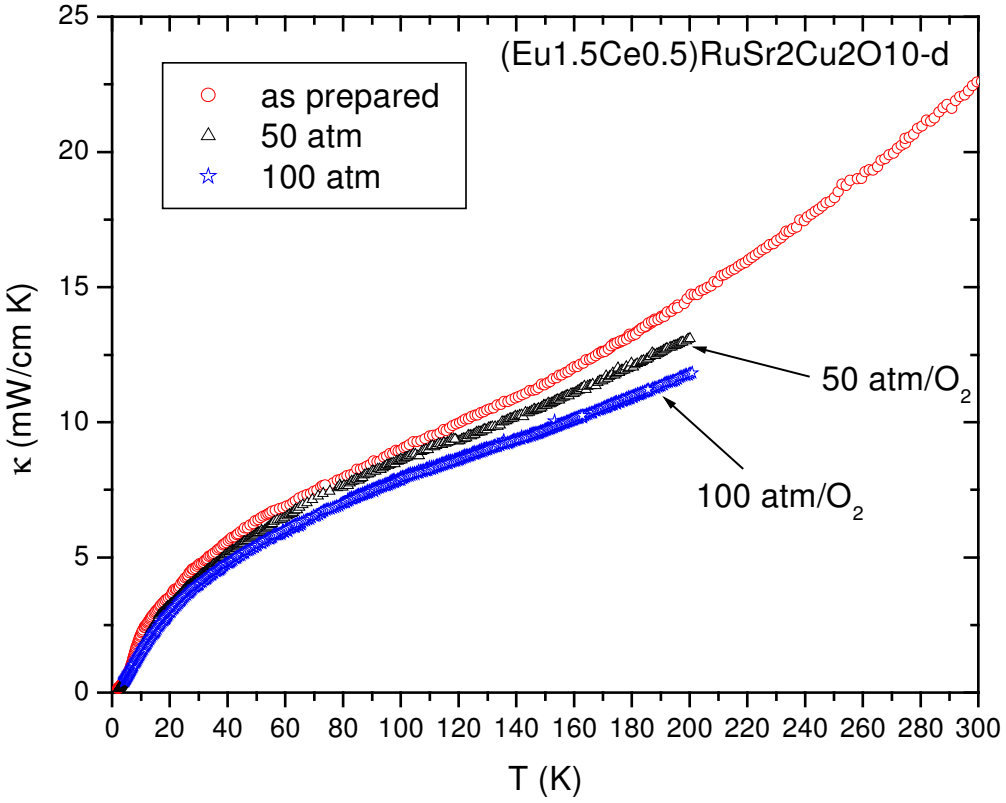

Figure 19. Thermal conductivity κ versus temperature T for $(Eu_{1.5}Ce_{0.5})RuSr_2Cu_2O_{10-\delta}$ samples with different oxygen content (as prepared, annealed at 50 atm/O_2 and annealed at 100 atm/O_2).

Figure 19 shows thermal conductivity versus temperature measured from 1.8K to 300K for the as-prepared sample and from 1.8K to 300K for samples annealed in oxygen. The thermal conductivity at high temperatures is approximately linear with temperature. The magnitude for thermal conductivity at room temperature is about

23 mW/cm*K for the as-prepared sample. At low temperatures thermal conductivity for the three samples is very close in magnitude. With the Wiedeman-Franz law one can approximately estimate the electron contribution to the thermal conductivity. The calculations for all three samples show that the biggest electron contribution is at room temperature and is less than 1% of the total thermal conductivity. This indicates that the phonons are major carriers of heat in these samples.

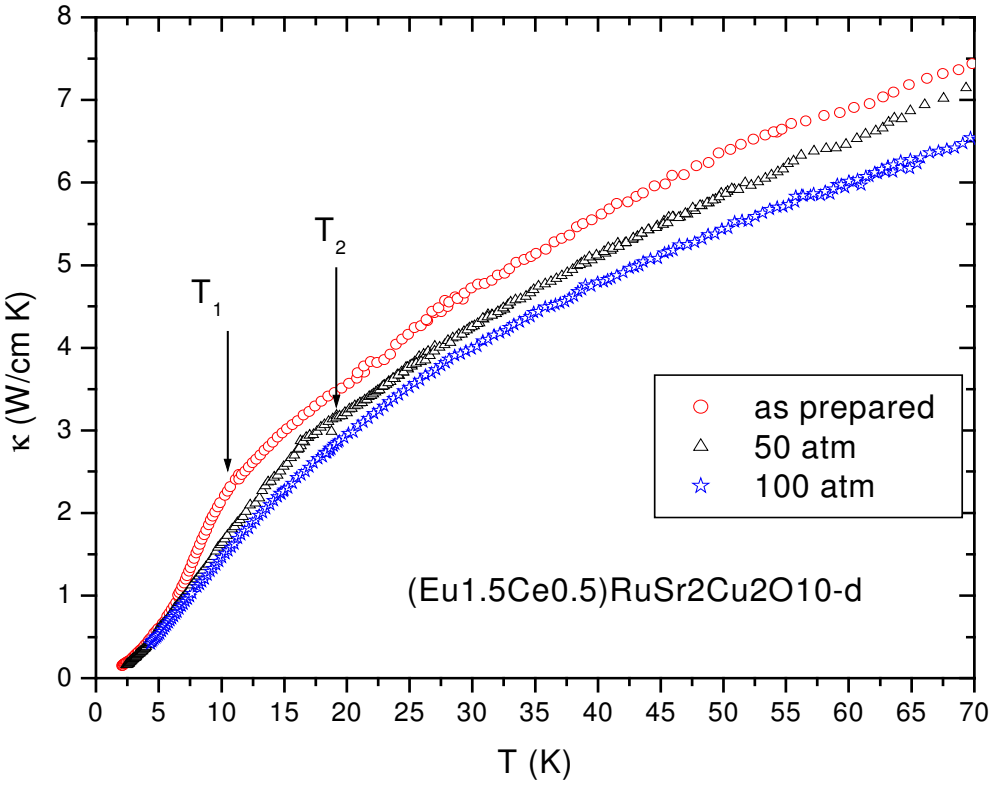

Figure 20. The expanded view of thermal conductivity versus temperature for $Eu_{1.5}Ce_{0.5})RuSr_2Cu_2O_{10-\delta}$ samples with different oxygen content (the samples as-prepared, annealed at 50 atm/O_2 and annealed at 100 atm/O_2).

Figure 20 shows an expanded view of the thermal conductivity versus temperature for all three samples of Ru-1222(Eu) at low temperatures. $\kappa(T)$ data does not show a clear indication of T_c for either sample. However there is a distinct change in the slope of $\kappa(T)$ at T_1 around 10K for the as-prepared sample and at T_2 around 19K for the sample annealed at 50atm. The sample annealed in oxygen at 100atm does not show a clear indication of such a shoulder feature at low temperatures.

The thermal conductivity for a Ru-1222(Eu) sample annealed at 54 atm/O_2 at 800^{o}C for 12 hours was reported earlier in [42]. The article reported an anomalous behavior of $\kappa(T)$ around 48K, which corresponds to the superconducting transition temperature T_c. The present data for $\kappa(T)$ (see Figures 19 and 20) do not show this abnormal behavior near the onset of superconductivity. However, the additional small shoulder feature in $\kappa(T)$ near 10K reported in [42] can also be observed in Figure 20 for the as-prepared sample and the sample annealed at 50 atm/O_2.

D. Resistivity Data for $(Gd_{1.5}Ce_{0.5})RuSr_2Cu_2O_{10-\delta}$

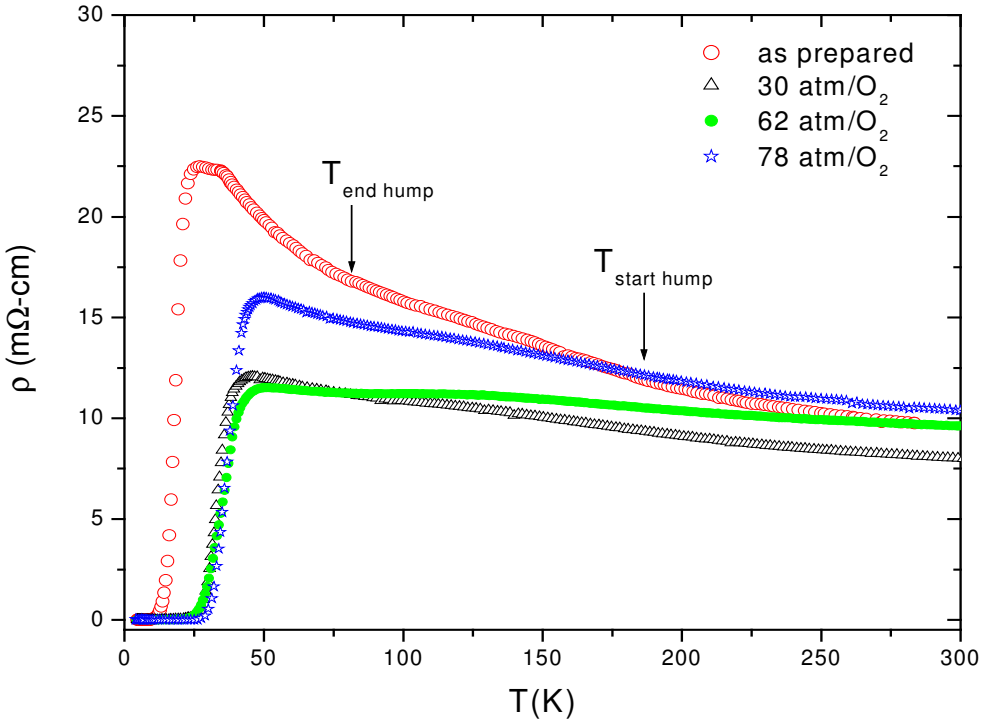

Figure 21. The resistivity of $(Gd_{1.5}Ce_{0.5})RuSr_2Cu_2O_{10-\delta}$ samples with different oxygen content (the as-prepared, annealed at 30, 62 and at 78 atm/O_2 samples).

Figure 21 shows the resistivity versus temperature of $(Gd_{1.5}Ce_{0.5})RuSr_2Cu_2O_{10-\delta}$ samples (Ru-1222(Gd)) with different oxygen content measured from 4K to 300K. All four samples exhibit semiconductor like behavior in different degrees of steepness with decreasing temperature. The as-prepared sample shows the steepest increase in resistivity with decreasing temperature. The sample annealed at 62 atm in oxygen shows the slowest increase in slope of ρ(T) with temperature. All four samples show what

appears to be a hump in the resistivity starting around 180K and ending around 80K ($T_{hump\ start}$ and $T_{end\ hump}$). The ρ(T) curves indicate the broad superconducting transition for all four samples. (For more discussion see Section IV, Subsection E).

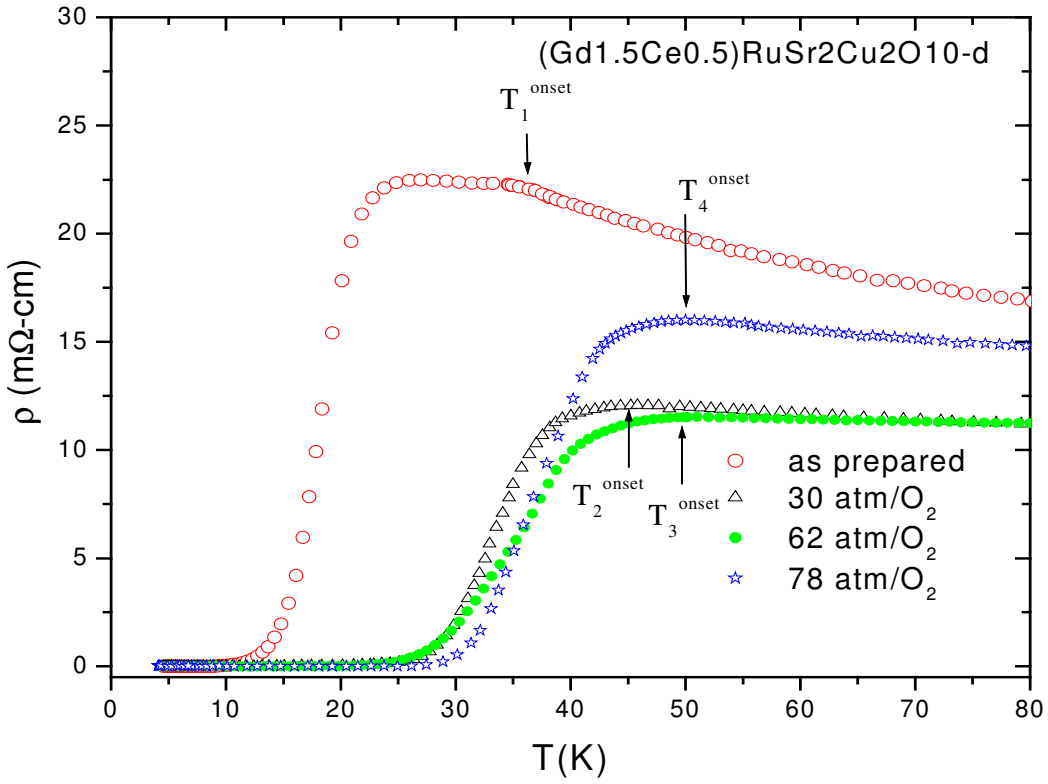

Figure 22. The expanded view for resistivity of $(Gd_{1.5}Ce_{0.5})RuSr_2Cu_2O_{10-\delta}$ samples with different oxygen content (the samples as-prepared, annealed at 30, 62, and 78 atm/O_2).

Figure 22 shows an expanded view of the electrical resistivity versus temperature for Ru-1222(Gd) samples annealed at different oxygen pressures. The arrows represent the temperature of onset of superconductivity for the different samples. The onset of superconductivity for the as-prepared sample is $T^{onset} \approx 36K$. T^{onset} for the sample

annealed at 30 atm/O_2 is around 45K. The sample annealed at 62 atm/O_2 has T^{onset}≈48K and the sample annealed at 78 atm/O_2 has T^{onset}≈50K. The onset of superconductivity, T^{onset} for all four samples were determined from the resistivity data (see Figure 22) at the temperature where the superconducting phase just emerges.

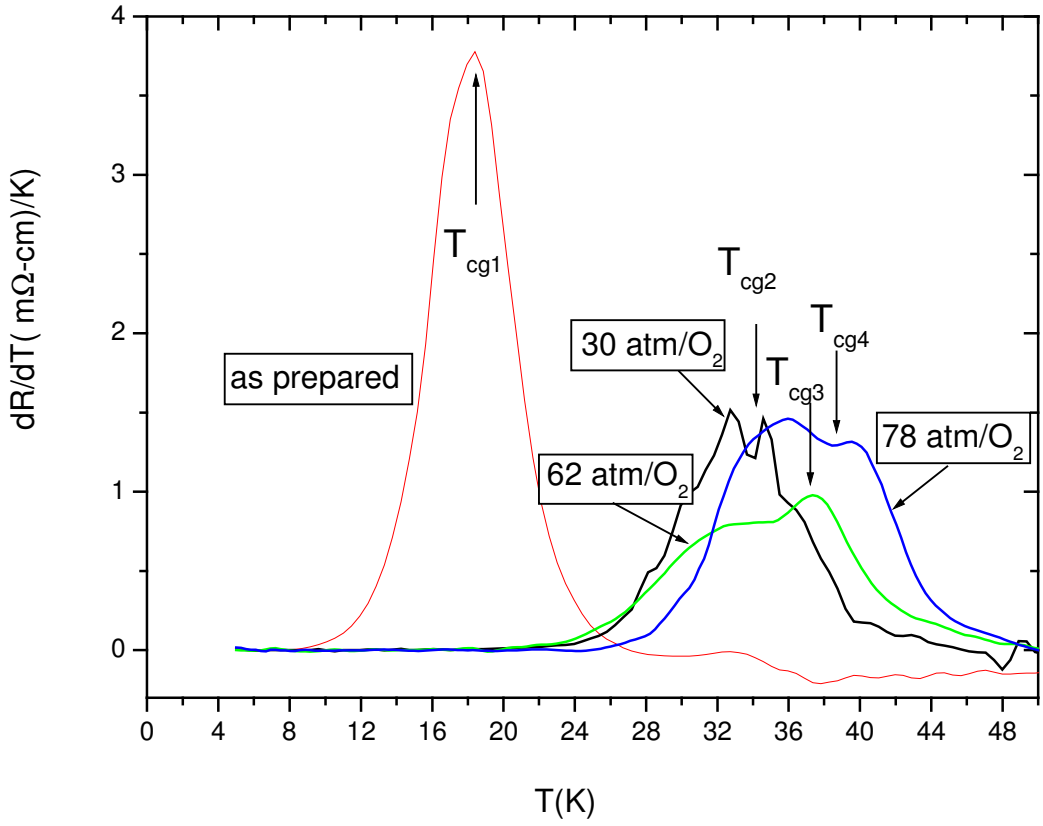

Figure 23. Derivatives dR/dT versus temperature for $(Gd_{1.5}Ce_{0.5})RuSr_2Cu_2O_{10-\delta}$ samples with different oxygen content (the samples as-prepared, annealed at 30, 62, and 78 atm/O_2).

Figure 23 shows the derivatives, dR/dT, for Ru-1222(Gd) samples with different oxygen content. All four samples exhibit two-step superconducting transition, which corresponds to two temperatures, T_c and T_{cg} (corresponding to intra-grain and inter-grain transition temperatures respectively). The as-prepared sample has a well-defined peak at $T_{cg1}\approx 19K$. All other samples have rather broad peaks corresponding to inter-grain transition temperatures T_{cg}. The thermopower data were used to determine T_{cg}-s more precisely (see Subsection E below). The position of intra-grain transition temperature T_c for all four samples cannot be precisely determined nether from resistivity data Figure 22 or 23 nor from thermopower data (see Figure 24 or 25). Thus T^{onset} can approximately correspond to the intra-grain transition temperature for all four samples. The complete data for T^{onset}, T_c and T_{cg} for all four samples are given further below in the table in Section IV, Subsection A. The intra-grain transition temperatures T_c are marked as question mark for the reason has just explained.

E. Thermopower Data for $(Gd_{1.5}Ce_{0.5})RuSr_2Cu_2O_{10-\delta}$

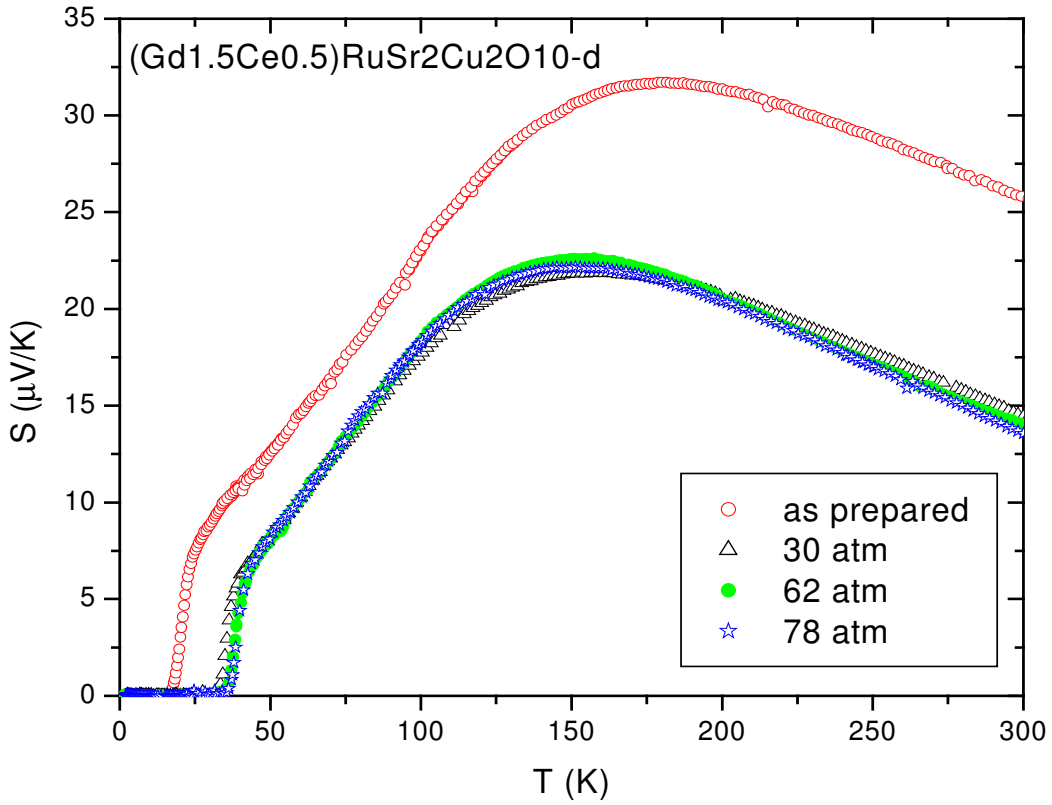

Figure 24. The thermopower versus temperature for $(Gd_{1.5}Ce_{0.5})RuSr_2Cu_2O_{10-\delta}$ sample with different oxygen content (the as-prepared, annealed at 30, 62, and 78 atm/O_2 samples).

Figure 24 shows the absolute thermopower for Ru-1222(Gd) samples with different oxygen content measured from 1.8K to 300K. All samples show rather large magnitude for the thermopower above T_c. The magnitude for the as-prepared sample is 33% bigger at low temperatures (above superconducting phase) and 46% bigger for high temperatures compared to the samples annealed in oxygen. The samples annealed in

oxygen have very similar values for the thermopower. The data for S(T) are similar in temperature dependence to that earlier reported in [43]. The thermoelectric power is positive for the entire temperature range, consistent with hole charge carriers [39, 42]. The room temperature value of S, i.e. S^{300K}, for the as-prepared sample is found to be approximately 26 μV/K. All four curves pass through a maximum (TEP maximum). The TEP maximum for the as-prepared sample is at approximately 170K. The TEP maximum for the samples annealed in oxygen is at about 140K. Annealing in oxygen seems to shift the TEP maximum to lower temperatures and to decrease its magnitude.

The general shape of S(T) curves for Ru-1222(Gd) is quite similar to that for Ru-1222(Eu) with the exception that the decrease to S=0 at T_c is much broader for Ru-1222(Eu). This suggests that the granularity effects are much more pronounced in Ru-1222(Eu), as does ρ(T) data. The similarity of S(T) curves for both Ru-1222(Gd) and Ru-1222(Eu) suggests that this characteristic behavior of S(T) may be universal in rutheno-cuprates.

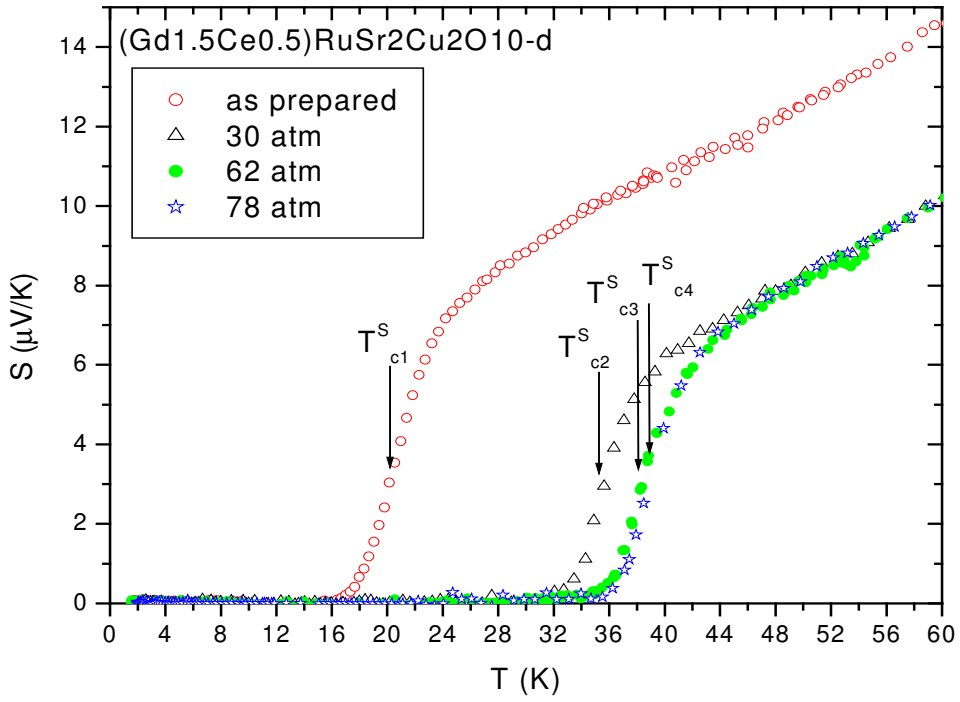

Figure 25. The expanded view of the absolute thermopower versus temperature for $Gd_{1.5}Ce_{0.5})RuSr_2Cu_2O_{10-\delta}$ samples with different oxygen content (the as-prepared, annealed at 30, 62, and 78 atm/O_2 samples).

Figure 25 shows an expanded view of the absolute thermopower versus temperature for Ru-1222(Gd) samples annealed at different oxygen content. The superconducting transition temperatures were determined from the first derivative, dS/dT. The complete list of superconducting temperatures T_c^S determined from S(T) data are given in the table in Section IV, Subsection A. These T_c^S agree well with the electrical resistivity data for T_{cg} shown in Figures 21-23 (see also the table in Section IV, Subsection A).

F. Thermal Conductivity Data for $(Gd_{1.5}Ce_{0.5})RuSr_2Cu_2O_{10-\delta}$

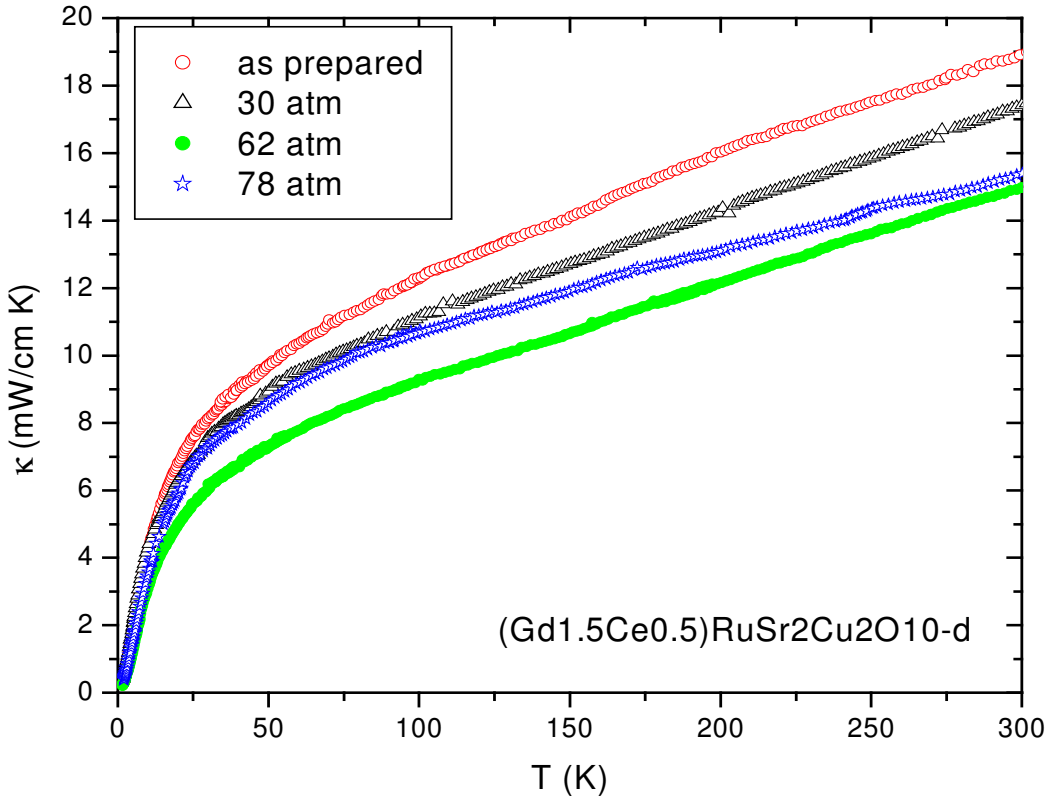

Figure 26. Thermal conductivity versus temperature for $(Gd_{1.5}Ce_{0.5})RuSr_2Cu_2O_{10-\delta}$ samples with different oxygen content (the as-prepared, annealed at 30, 62, and 78 atm/O_2 samples).

Figure 26 shows the thermal conductivity versus temperature for Ru-1222(Eu) samples with different oxygen content measured from 1.8K to 300K. The thermal conductivity at high temperatures is approximately linear with temperature. The magnitude for the thermal conductivity at room temperature is about 19 mW/cm*K for

the as-prepared sample. The samples annealed in oxygen have slightly lower thermal conductivity. At low temperatures, the thermal conductivity of all four samples is very close in magnitude. With the Wiedeman-Franz law, it was found that the electron contribution to the thermal conductivity is around 4% of the total thermal conductivity. That indicates that the phonons are major carriers of heat.

Figure 27 shows an expanded view of the thermal conductivity versus temperature for all four samples at low temperatures. The κ (T) data do not show a clear indication of T_c for either sample. The thermal conductivity increases monotonically with temperature. (For more detailed discussion see Section IV, Subsection C).

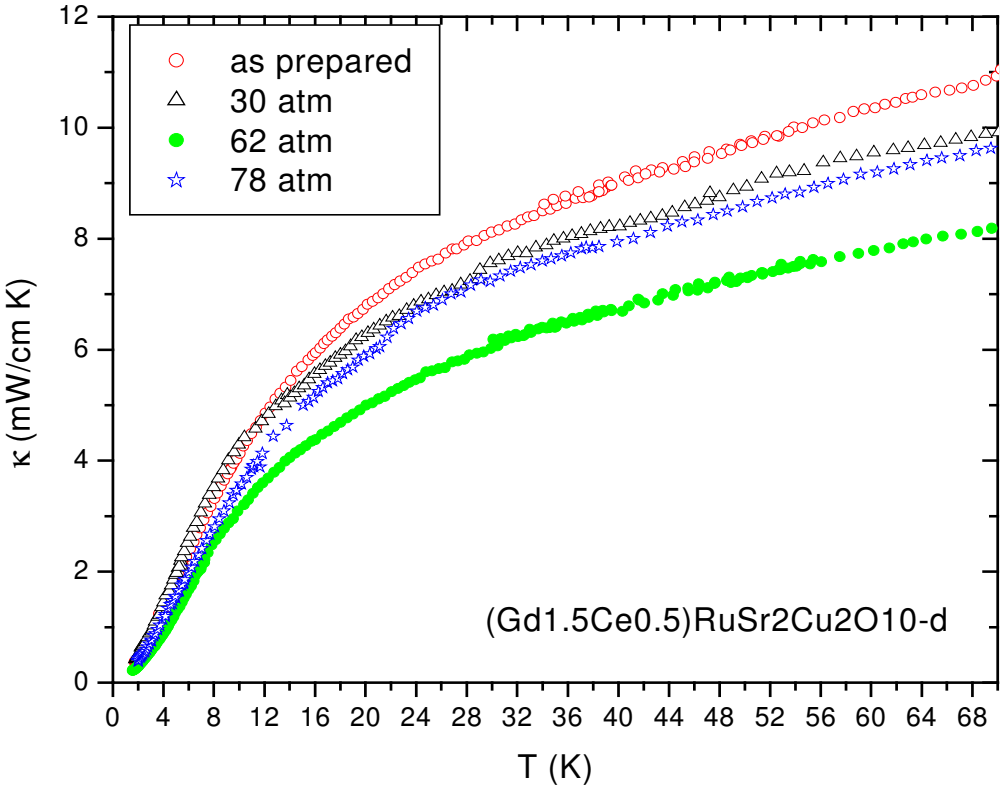

Figure 27. The expanded view of thermal conductivity versus temperature for $(Gd_{1.5}Ce_{0.5})RuSr_2Cu_2O_{10-\delta}$ sample with different oxygen content (the as-prepared, annealed at 30, 62, and 78 atm/O_2 samples).

IV DISCUSSION

A. Resistivity

Table 1 and Table 2 list the values for onset of superconductivity as well as the temperatures for intra-grain (T_c) and inter-grain (T_{cg}) superconducting transitions for Ru-1222(Eu) and Ru-1222(Gd) samples with different oxygen content.

Table 1. The onset of superconductivity and the values for first and second superconducting temperatures, T_c and T_{cg} superconducting temperatures for Ru-1222(Eu) with different oxygen content.

	As-prepared	50 atm/O_2	100 atm/O_2
T_c (K)	39	45	44.5
T_{cg} (K)	10	20	21.5
T^{onset}~T_c (K)	39	45	44.5

Table 2. The onset of superconductivity, the values for first and second superconducting temperatures, T_c and T_{cg} determined from resistivity data and the superconducting temperatures T_c^S determined from thermopower data for Ru-1222(Gd) with different oxygen content.

	As-prepared	30 atm/O_2	62 atm/O_2	78 atm/O_2
T^{onset}	36	45	48	50
T_{cg}	19	~34	~37	~38
T_c (K)	?	?	?	?
T_c^S	20	35	38	38.7

The results from Table 1 and Table 2 show that the increase in oxygen content shifts the temperature of superconducting transition to higher temperatures. At the same time, from Figures 16 and 21 we can see that there is no consistent decrease in resistivity values with increasing oxygen content as was previously reported in [41]. Comparison of the resistivity of the as-prepared sample and samples annealed in oxygen shows that the increase in oxygen content decreases the resistivity in oxygen-doped samples. However, comparison of the resistivity of the oxygen-doped samples indicates that the highest value for resistivity is for the sample annealed at the highest oxygen pressure. In earlier works [38, 44, 45] it was shown that the increase in oxygen content decreases the resistivity in the normal state. The decrease in resistivity can be explained by the fact that the increase in the oxygen doping, increases the average hole density (p) in the CuO_2 planes, which are believed to be responsible for superconductivity [45]. A study of influence of the oxygen content and effect of aging are presented in [41], which explained the deterioration of the samples in a period of a few months and their recovery after annealing in a high-pressure atmosphere of oxygen. This study showed that with aging, in a polycrystalline sample, the oxygen first leaves the grain boundaries, thus strongly affecting the magnitude of resistivity of the sample. Further reduction in the oxygen content was observed to reduce oxygen in the RuO_2 planes, strongly affecting the magnetic order and leading to a spin glass phase. In the aging process further oxygen depletion removes oxygen from the CuO_2 planes, gradually suppressing the superconductivity. The recovery re-oxidation process is similar and reverse to aging. When the sample is re-annealed in oxygen this leads to a quick recovery in the resistivity

of the sample because the grain boundaries are easily oxygenated. However, the oxygen diffusion inside grains is a more complicated process [38, 44, 45]. By further increase of the oxygen content, oxygen begins to diffuse into the CuO_2 planes of the superconducting grains and superconductivity begins to recover.

The samples used in our studies were prepared in Israel and did not arrive in our lab until several weeks after preparation. In that time, it appears that diffusion of oxygen from the grain boundaries for the Ru-1222(Eu) and Ru-1222(Gd) samples annealed at 100 atm and 78 atm respectively, was more than for those samples annealed at lower oxygen pressure, leading to higher resistance for the samples annealed at higher oxygen preassures. Thus the oxygen content of Ru-1222 samples can change with time and that aging process may be the origin for many discrepancies between results reported in the literature.

B. Granularity Effect in the Rutheno-Cuprates

Figure 16 and Figure 21 show that all samples exhibit a superconducting transition. It is apparent that the superconducting transitions are much broader than those observed in many other high T_c superconductors. This transition width is comparable to the results found in the literature [46] for the Ru-1222 family, however. There are two hypotheses to explain this. The first explanation, proposed in [45], suggested that this relatively broad transition might be a characteristic of coupled magnetic superconducting state identified as the spontaneous vortex phase discussed in detail in [47]. Measurements done by means of magneto-optical imaging [47] were interpreted as

possible evidence for the spontaneous vortex phase (SVP), which assumes that in weak-ferromagnetic superconducting materials vortices are present in the sample in equilibrium without an external magnetic field. The results of this experiment showed that the saturation moment of the Ru sublattice created an internal field (higher than H_{c1}) of a few hundreds of G, which might induce vortices in the superconducting plane. The spatial resolution of the experiment was not sufficiently good to resolve vortices, however. Consequently, a second explanation must be considered at least equally as likely.

The second explanation of the broad superconducting transition is the granular nature of this material. For the polycrystalline structure with a grain size of a few μm the superconducting transition may occurs via two intermediate stages [48]. Nonhomogeneous oxygen distribution can cause oxygen depletion of the grain-boundary regions and, hence, weak electrical connectivity between the grains [49]. The broadening of the resistive transition was already observed in oxygen annealed Ru-1222 materials, and was related to inhomogeneity in the oxygen concentration [41]. A two-step transition appears due to the transition of the individual superconducting grains at a rather well defined temperature T_c (intra-grain superconducting temperature). At lower temperature Josephson tunneling can couple the different grains over macroscopic distances. Inter-grain phase coherence is then established at $T_{cg.}$ The step-like transition due to weak Josephson inter-grain coupling is affected dramatically by the applied field and value of the electrical current [49, 50]. A more detailed theoretical description of behavior of superconductivity in inhomogeneous systems can be found in [48].

Our data suggest the granular nature of superconducting Ru-1222 samples. A two stage superconducting transition is clearly observed for all three of Ru-1222(Eu) and four of Ru-1222(Gd) samples. The intra-grain sharp drop of the resistivity at T_c^{onset} occurs when the grains become superconducting. At this point the weak links between the grains contribute non-zero resistance across the sample. At lower temperatures the weak-links between grains become superconducting through Josephson tunneling. An inter-grain transition temperature T_{cg} can be defined in terms of phase coherence over macroscopic distances. The derivative curves on Figure 18 clearly show the two peaks denotes as T_c and T_{cg}, corresponding to intra-grain and inter-grain critical temperatures, respectively. From our resistive data we can see that annealing in oxygen shifts the two transition temperatures closer to each other and suppreses the shoulder. For example, in the as-prepared Ru-1222(Eu) sample, the distance between the T_{c1} and T_{cg1} is around 30K but for the Ru-1222(Eu) samples annealed in oxygen this temperature difference corresponds to only about 25 K. At the same time, the Ru-1222(Eu) as-prepared sample has a more defined shoulder compared to the other two samples annealed in oxygen. Thus it is seen that intra-granular superconducting properties are much less affected by the high-pressure oxygen annealing than the inter-granular ones.

The intra-grain transition is not as dramatic, but still present in Ru-1222(Gd) samples. The as-prepared Gd sample has a rather flat resistive curve between the intra-grain T_c and inter-grain T_{cg} temperatures. The inter-grain temperature for the as-prepared and samples annealed in oxygen are shown as T_{cg}-s in Figure 23. The intra-grain temperatures are not denoted in Figure 23 because they cannot be determined precisely

neither from the resistivity data nor from thermopower data but they can be approximately assigned to the temperature of the onset of superconductivity.

By comparing the derivatives of Ru-1222(Eu) samples (see Figure 17), we can notice that the process of annealing in oxygen affects the intra-grain transition much less than the inter-grain superconducting transition. On one hand, the annealing shifts both the intra-grain and inter-grain transition temperatures to the higher temperatures. On the other hand, the annealing also depresses the peak in dR/dT corresponding to the inter-grain transition (T_{cg}) more than it does for intra-grain transition. This phenomenon may be explained by the fact that, during the annealing in pure oxygen, the grain boundaries are oxygenated more easily thus strongly affecting the resistivity of the sample and the shape of the shoulder in the inter-grain superconducting transition. This fact can also be observed in [40, 41].

The change in grain structure with annealing for Ru-1222(Gd) samples is more complex. First, we notice that the annealing does not affect the intra-grain transition temperature (which approximately corresponds to the onset of superconductivity) as strongly as for Ru-1222(Eu). At the same time the inter-grain transition temperature shifts to higher temperatures for annealed Ru-1222(Gd) samples.

It is interesting to compare the annealed samples. In Ru-1222(Eu) samples, the sample annealed in 50 atm/O_2 has a slightly higher intra-grain transition temperature (T_c) and slightly smaller shoulder in the inter-grain transition (T_{cg}) than the sample annealed in 100 atm/O_2. This fact may be explained by the process of aging. Because of the storage, oxygen not only depleted from the grain boundaries in 100 atm/O_2 sample, thus

strongly affecting the resistivity of this sample and the shape of the shoulder in the inter-grain superconducting transition T_{cg} but also partially left the grains thus affecting the temperature of the intra-grain superconducting transition T_c in that sample.

For Ru-1222(Gd) samples, the sample annealed in 78 atm/O_2 has higher intra-grain and inter-grain transition temperatures than samples annealed in 62 atm/O_2 and 30 atm/O_2. But at the same time, 78 atm/O_2 sample also has a more defined shoulder (corresponding to the inter-grain transition) and the highest resistivity. Dealing with the fact that, the sample with 78 atm/O_2 was the last one measured, we can conclude that because of aging this sample lost mainly oxygen from grain boundaries (thus affecting the resistivity of the sample and the shape of the shoulder in the inter-grain superconducting transition) and left the composition inside the grain mostly unaffected. This proposition is supported by the study of Lorenz, et. al. [40]. In this article, the synthesis and physical properties of ferromagnetic $RuSr_2GdCu_2O_8$ were investigated. Comparing four samples, the as-prepared, annealed in oxygen, annealed in air and annealed in argon, they found that annealing in air and argon strongly degraded the grain boundaries and thus inter-grain coupling while barely affecting the intra-grain transition [40]. Thus taking into account the earlier research on the process of annealing and aging we can support the suggestion that the Ru-1222(Gd) samples lost oxygen mainly from the grain boundaries and left the composition inside the grains unchanged, and thus the intra-grain superconducting transition temperature unaffected.

Summarizing, from the resistivity data for Ru-1222(Gd) and Ru-1222(Eu) samples we can make two conclusions. First, our data show that the process of aging

affects not only the magnitude of resistivity in normal state but also the shape of the shoulder in the superconducting transition. This is strong evidence supporting the oxygen deficiency as the main source of granularity. Additional deoxydation of the samples occurs during storage, causing granularity effects to be more pronounced [50] after further aging.

Second, the process of deoxydation goes faster for Ru-1222(Eu) samples than for Ru-1222(Gd) samples. This conclusion is supported by the fact that when comparing annealed Ru-1222(Gd) and Ru-1222(Eu) samples, we observe that the Ru-1222(Eu) sample annealed at the highest pressure shows not only an increase in the normal state resistivity, but also a very slight decrease of the intra-grain transition temperature (T_c in Table 1) of superconductivity. By contrast, the aged Ru-1222(Gd) sample annealed at the highest pressure shows only an increase in normal state resistivity but still has the highest intra-grain T_c among the other Ru-1222(Gd) samples.

C. Thermal Conductivity

The thermal conductivity data shown in Figure 19 and Figure 26 for Ru-1222(Eu) and Ru-1222(Gd) are unique data except for the measurement that was done on one of the Ru-1222(Eu) samples in our lab. These data can be found in [42]. The data on Ru-1222(Eu) samples (shown in Figure 19) do not conform to the features around T_c and transitions to the ferromagnetic state found in [42], but that was the first sample of these oxides we measured in our lab, and may have had a larger electronic contribution

to κ(T) than these later samples. The sample in [42] was accidentally warmed to 300K and left in vacuum at the completion of thermal properties measurements. Due to depletion of oxygen, its properties had changed before ρ(T) could be measured.

Comparing the κ(T) for Ru-1222(Eu) and Ru-1222(Gd) samples we can notice that in general the lower oxygen concentration gives the highest κ(T) values. Nevertheless, there are some discrepancies for the Ru-1222(Gd) sample annealed in 78 atm/O_2. Since no other data are available for the comparison of the influence of oxygen content on the thermal conductivity of the Ru-1222(Eu, Gd), we can use for comparison the thermal conductivity of the high T_c polycrystalline samples of $EuBa_2Cu_3O_{7-\delta}$ which are described in [51, 52]. In these references, a non-monotonic oxygen-doping dependence of κ(T) for $EuBa_2Cu_3O_{7-\delta}$ samples was found. The explanation for this behavior was given in the context that thermal conductivity not only depends on temperature and oxygen content, through the charge carriers and phonons and their interactions, but apparently it could depend as well on the oxygen ordering through the sample [51-53]. Since the Ru-1222(Eu) and Ru-1222(Gd) samples have a granular nature, which suggests non-homogeneous oxygen distribution through the sample, this may be the reason for the non-monotonic behavior of κ(T) versus oxygen content observed here. The sample that gives the deviation from monotonic dependence on the annealing pressure is the sample that was annealed in 78 atm/O_2, which also showed a deviation in resistivity data (see Figures 19 and 26). The explanation for the resistivity discrepancy was the aging process, which caused the granular effects (and consequent oxygen inhomogeneity) to be more pronounced.

The relative contribution to the thermal conductivity by electrons and phonons was estimated by using the Wiedemann-Franz relation (4) and the resistivity data.

$$\kappa_e(T) = LT\sigma(T) \quad (4)$$

where $L=2.44\times10^{-8}$ W Ω/K^2 is the Lorenz number, σ is the electrical conductivity, T is temperature, and κ_e is the thermal conductivity due to electrons.

The calculation showed that the maximum electron contribution for Ru-1222(Eu) is about 0.75% and that for Ru-1222(Gd) samples is around 4 %. These results show that nearly all of the heat is transferred by lattice vibrations (phonons). The contribution to the total thermal conductivity by electrons becomes more significant for the samples with the highest concentration of oxygen.

Table 3. Relative contribution to the total thermal conductivity by electrons at 300 K, $\kappa_e(\%)HT$, and near the superconducting temperature 50 K, $\kappa_e(\%)T_c$, for Ru-1222(Eu) samples with different oxygen concentrations.

	As-prepared	50 atm/O_2	100 atm/O_2
$\kappa_e(\%)HT$	0.73	~ 0.73	~ 0.73
$\kappa_e(\%)T_c$	0.074	0.136	0.139

Table 4. Relative contribution to the total thermal conductivity by electrons at 300K, $\kappa_e(\%)HT$, and near the superconducting temperature 50K, $\kappa_e(\%)T_c$, for Ru-1222(Gd) samples with different oxygen concentrations.

	As-prepated	30 atm/O_2	62 atm/O_2	78 atm/O_2
$\kappa_e(\%)HT$	4.28	5.23	5.42	4.49
$\kappa_e(\%)T_c$	0.61	1.13	1.48	0.89

Table 3 and Table 4 show the relative contribution to the total thermal conductivity, $\kappa = \kappa_e + \kappa_{ph}$, by electrons at high temperatures, $\kappa_e(\%)HT$, and near the superconducting temperature, $\kappa_e(\%)T_c$, for Ru-1222(Eu) and Ru-1222(Gd) samples with different oxygen concentrations. The tables show that the most resistive sample, which corresponds to the as-prepared sample, shows the lowest electron contribution at high and low temperatures. This observation agrees with the results for Y-123 and Eu-123 reported in [51-53].

Those electrons that are condensed into Cooper pairs are not able to carry entropy and therefore they do not carry heat. For this reason one would hope that the changes to the superconducting state would affect the mechanism of conduction of heat and consequently see the changes in $\kappa(T)$ curves near T_c. But because of the small electron contribution to the total thermal conductivity for Ru-1222(Gd) and Ru-1222(Eu) samples the change near the T_c transition temperature is below the experimental resolution.

Both Ru-1222(Gd) and Ru-1222(Eu) samples, show the increase of the thermal conductivity with temperature. This behavior is unexpected because in simple crystals the thermal conductivity due to phonons behaves as $\kappa=(1/3)C_p\lambda\nu$, [60, 2], where C_p is the lattice specific heat per unit volume, ν is sound velocity and λ is the scattering length. At high temperatures, C_p usually saturates and the scattering length decreases for phonon-phonon interactions, so one can expect that the thermal conductivity also decreases like in [51-52]. The specific heat measurements on Ru-1222(Gd) and Ru-1222(Eu) samples were performed in our lab. These unpublished preliminary data show the monotonic increase of the specific heat with temperature for both Ru-1222(Gd) and Ru-1222(Eu) compounds, which may explain the increase of the thermal conductivity with temperature.

In conclusion, the measured data for the total thermal conductivity for rutheno-cuprates do not show a strict monotonic oxygen-doping dependence of $\kappa(T)$ suggesting that it has sensitivity not only to oxygen concentration but also to the oxygen ordering. Further research is needed to investigate the dependence of oxygen content in Ru-1222(Eu) and Ru-1222(Gd) samples and its relation to the oxygen ordering.

D. Thermopower

The total thermopower is the sum of three contributions [33, 32, 57]

$$S(T)=S_d(T)+S_g(T)+S_m(T) \qquad (5)$$

where S_d is a diffusion contribution, which is related to the temperature dependence of the diffusion of the carriers to the cold end of a sample, and S_g is a phonon drag contribution resulting from the transfer of phonon momentum to the electron gas. As a result, due to the temperature gradient, the phonons on their way to the cold side of the sample "drag" electrons, thus giving an increase in the total thermopower at temperatures near $\theta_D/10$. The magnitude of the phonon drag component in metals generally rises as T^3 below $\theta_D/10$, reaches its maximum at about $\theta_D/10$ temperature, and falls as T^{-1}[32, 33]. If magnetic effects are present (such as magnetic impurities), the additional S_m term to the total S(T) can be present.

Classically, for metals or semiconductors, the thermopower is strongly influenced by the velocity of electrons at the Fermi level that varies with the compound. As a result the thermopower is also expected to be strongly dependent on the composition of the sample. However, in many experiments the thermopower of high T_c cuprates does not depend on the particular compound qualitatively and varies in a systematic manner according to the hole carrier concentrations [54]. This highly systematic behavior has been used very effectively as a guide for searching for samples with optimal doping [55].

According to Trodahl [56], the observed thermopower for high T_c superconductors is a sum of a negative diffusion thermopower $S_{d,}$ varying linearly in temperature and a positive phonon-drag thermopower S_g varying little in temperature above 100K (in contrast to the usual metallic behavior [32, 33]). Based on [56], S_d can be obtained by measuring the slope of the total measured thermopower at high

temperatures and multiplying by temperature T. By taking the difference between S_d and the total thermopower, one can obtain the thermopower due to the phonon drag. Figure 28 and Figure 29 show contributions to the total thermopower versus temperature due to diffusion S_d, and due to phonon drag S_g, respectively, for Ru-1222(Gd) samples based on Trodahl model.

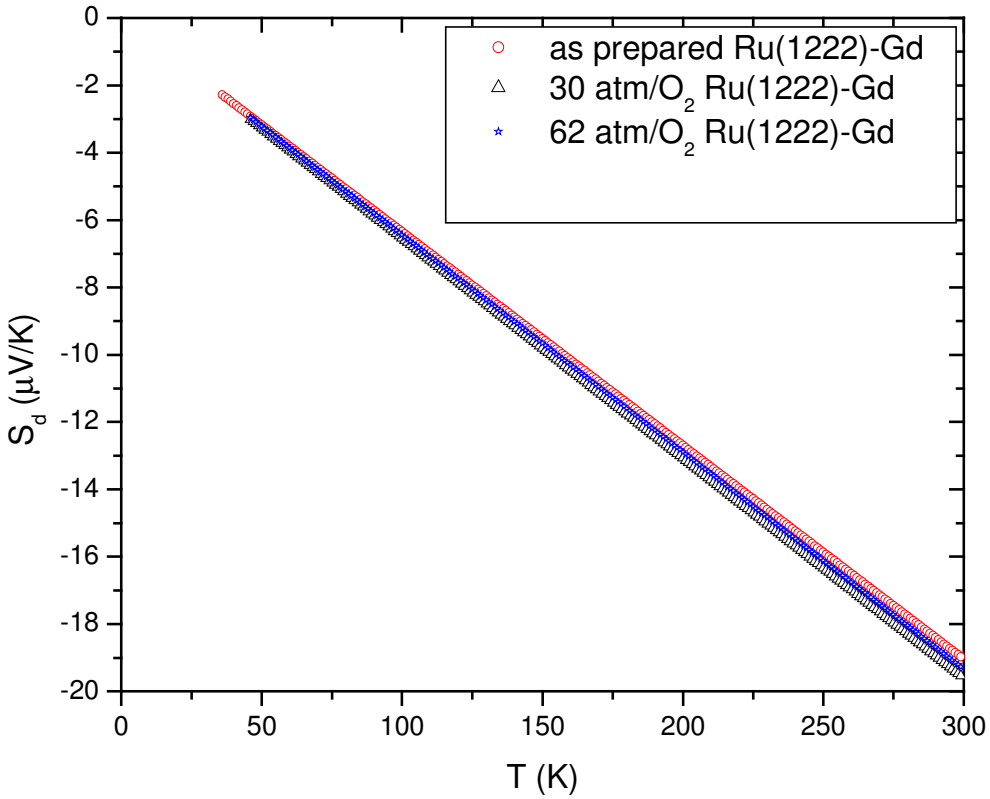

Figure 28. The diffusion thermopower versus temperature for Ru-1222(Gd) samples with different oxygen content.

Figure 28 shows that S_d determined from Trodahl's analysis [56] is almost independent of the hole doping, i.e. on annealing in oxygen. The as-prepared sample has almost the same slope as the samples annealed in oxygen. Note that this result is in contradiction with the Mott formula at high temperatures [32, 57], i.e.

$$S_d(T) \approx (280\mu V/K)(kT/E_F) \qquad (6)$$

where E_F is the Fermi energy, k is the Boltzmann constant, and T is temperature.

On one hand, the annealed sample has more hole-carriers than the as-prepared one; consequently, since the Fermi energy increases with the number of carriers, S_d must noticeably vary with the hole concentration (see formula (6)). On the other hand, the Mott formula is for 3-D systems; the Ru-1222(Gd) and Ru-1222(Eu) are strongly inhomogeneous samples due to their granular structure, and grains are more 2-D like which would change the dependence of the Fermi energy on the number of carriers.

The number of holes per CuO_2 plane p (see below) estimated from formula (7) shows that p does not change much with annealing, i.e. from 0.095 holes/CuO_2 in the as-prepared sample to 0.112 holes/CuO_2 in sample annealed at 78 atm/O_2. This may explain why S_d only slightly depends on the hole doping in Figure 28.

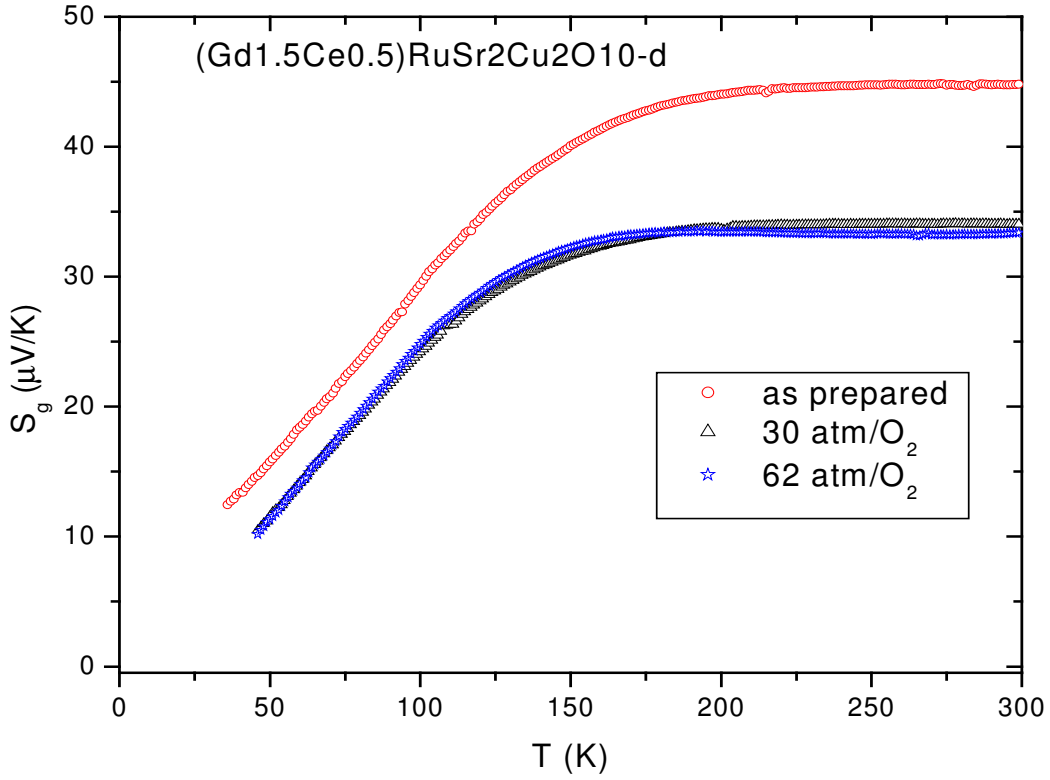

Figure 29. The phonon drag thermopower versus temperature for Ru-1222(Gd) samples with different oxygen content.

Figure 29 shows the phonon drag thermopower S_g versus temperature for Ru-1222(Gd) samples with different oxygen content. Figure 29 shows the systematic shift of the saturation value of S_g at high temperatures toward lower values with increasing concentrations of holes, which is in agreement with [43]. The literature indicates, this relationship is nearly universal in these materials and S_{290K} has been used as a gauge of hole concentrations [55, 56, 58].

To estimate the hole concentration per CuO_2 planes, p, the proposed correlation (7) was used [55].

$$S_{290K} = (992\ \mu V/K)\ \exp(-38.1\ p) \qquad (7)$$

The estimates of p for Ru-1222 (Gd) using formula (7) were compared in [43] to determinations by using a gas-effusion cell and found to be in agreement.

Table 5 shows the hole concentration, p, for the as-prepared sample and samples annealed in oxygen at 30, 62, and and 62 atm/O_2 for the Ru-1222(Gd) compound estimated from formula (7).

Table 5. The hole concentration, p, for the as-prepared sample and samples annealed in oxygen at 30, 62, and 78 atm/O_2 for Ru-1222(Gd) compound.

	As-prepared	30 atm/O_2	62 atm/O_2	78 atm/O_2
p (per CuO_2)	0.095	0.110	0.111	0.112

The results show an increase in concentration, p, from 0.095 holes/CuO_2 in the as-prepared sample to 0.112 holes/CuO_2 in the sample annealed at 78 atm/O_2. These results agree with those reported in [43]. A similar analysis for the as-prepared Ru-1222(Eu) sample gives a value for p of 0.076 holes per Cu/O_2 plane. This much smaller value is also indicative of the greater sensitivity of the Ru-1222(Eu) compound to oxygen loss.

E. Magnetism in Ru-1222(Gd) and Ru-1222(Eu)

The thermopower and thermal conductivity data for Ru-1222(Gd) and Ru-1222(Eu) do not indicate the magnetic transitions near critical temperatures. The electrical resistivity data for all samples indicate a small hump in the data starting around 180 K and ending around 70 K. It is interesting to note that those two temperatures approximately correspond to the antiferromagnetic and ferromagnetic transitions, respectively. The upward hump may be the indication of the magnetic transitions around these temperatures [59, 17]. This conjecture is supported by the investigation of resistivity versus magnetic field in [59], which showed the suppression of a similar hump in a magnetic field. The resistivity data for Ru-1222(Eu) and Ru-1222(Gd) in Figure 16 and Figure 21 also show a slight suppression of this feature with oxygen annealing.

V CONCLUSIONS

In this work the influence of the oxygen content on the thermal and electrical properties of polycrystalline samples of Ru-1222(Gd) and Ru-1222(Eu) was studied.

The resistivity data show that the process of annealing in oxygen results in a decrease in normal state resistivity, an increase of the superconducting transition temperature and suppression of the two step-superconducting transition, which reveals the granular nature of the Ru-1222(Gd) and Ru-1222(Eu) samples.

The data for the total thermal conductivity for Ru-1222(Gd) and Ru-1222(Eu) do not show a strict monotonic oxygen-doping dependence for $\kappa(T)$ suggesting that it has sensitivity not only to the oxygen concentration but also to the oxygen distribution. Further research is needed to investigate the dependence of oxygen content in Ru-1222(Eu) and Ru-1222(Gd) samples and its relation to the oxygen distribution.

The relative contribution to the thermal conductivity by electrons and phonons was estimated by using the Wiedemann-Franz relation and resistivity data. The estimate showed that the maximum electron contribution for Ru-1222(Gd) samples is around 4 %. Thus nearly all of the heat is transferred by lattice vibrations (phonons). The contribution to the total thermal conductivity by electrons becomes more significant for the samples with the highest concentration of oxygen.

The data for the absolute thermopower indicate that oxygen doping results in a decrease of the absolute thermopower. Room temperature values of thermopower were used to estimate the hole concentration in the samples.

The possible effect of the presence of magnetism in Ru-1222(Gd) and Ru-1222(Eu) was only observed in the resistivity data. The small enhancement in the magnitude of the resistivity seen between 70 K and 180K may be related to ferromagnetic and antiferromagnetic transitions around those temperatures.

REFERENCES

[1] Doss J D 1989 *Engineer's Guide to High-Temperature Superconductivity* (New York: John Wiley & Son, Inc.)

[2] Gersten J I, Smith F W 2001 *The Physics and Chemistry of Materials* (New York: John Wiley & Son, Inc.)

[3] Мнеян М Г 1991 *Сверхпроводники в современном мире* (Москва: Посвещение) (Mnean M G 1991 *Contemporary superconductors* (Moskow: Posveshenie))

[4] Rjabinin J N, Schubnikov L V 1935 *Physikalishe Zeitschrift der Sowjetunion* **6** p 605

[5] Ginzburg V L, Andryushin E A 2004 *Superconductivity* (Singapore: River Edge, New York: World Scientific Publishing Co.)

[6] Burns G 1992 *High-temperature Superconductivity: An Introduction* (Boston: Academic Press, Inc.)

[7] Maple M B 1986 Novel types of superconductivity in f-electron systems *Physics Today* **March** p 72

[8] Moeno Y, Rice T M, Sigrist M 2001 The Intriguing Superconductivity of Stroncium Ruthenate *Physics Today* **January** p 42

[9] Levi B G 1993 In High-T_c Superconductors, is d-wave the new wave? *Physics Today* **May** p 17

[10] Levi B G 2002 Magnetism and Superconductivity Fight for Control in High-Tc Superconductors *Physics Today* **February** p 14

[11] Levi B G 2004 New Experiments Highlight Universal Behavior in Copper Oxide Superconductors *Physics Today* **September** p 24

[12] Mazin I I, Singh D J 1999 Competition in Layered Ruthenates: Ferromagnetism versus Antiferromagnetism and Triplet versus Singlet Pairing *Phys. Rev. Lett.* **82** p 4324

[13] Bauernfeind L, Widder W, Braun H F 1995 Ruthenium-based layered cuprates $RuSr_2LnCu_2O_8$ and $RuSr_2(Ln_{1+x}Ce_{1-x})Cu_2O_{10}$ (Ln=Sm, Eu and Gd) *Physica C* **254** p 151

[14] Bauernfeind L, Widder W, Braun H F 1995 *High T_c superconductors* of Forth Euro Ceramics **6** p 329

[15] Felner I, Asaf U 1997 Superconductivity and weak ferromagnetism in $Eu_{1.4}Ce_{0.6}Ru_{1-x}Fe_xSr_2Cu_2O_{10-\delta}$ *Physica C* **292** p 97

[16] Felner I, Asaf U, Levi Y, Millo O 1997 Coexistence of magnetism and superconductivity in $R_{1.4}Ce_{0.6}RuSr_2Cu_2O_{10-\delta}$ (R=Eu and Gd) *Phys. Rev. B* **55** p R3374

[17] Bernhard C, Tallon J L, Niedermayer Ch, Blasius Th, Golnik A, Brücher E, Kremer R K 1999 Coexistence of ferromagnetism and superconductivity in the hybrid ruthenate-cuprate compound $RuSr_2GdCu_2O_8$ studied by muon spin rotation and dc magnetization *Phys. Rev. B* **59** p 14099

[18] Tallon J L, Bernhard C, Bowden M, Gilbert P, Stoto T, Pringle D 1999 Coexisting ferromagnetism and superconductivity in hybrid rutheno-cuprate superconductors IEEE Transactions on Applied Superconductivity **9/2** p 1696

[19] Poole C P, Datta T, Farach H A 1988 *Copper Oxide Superconductors* (New York: John Wiley & Son, Inc.)

[20] Felner I 2002 Coexistence of Superconductivity and Weak-Ferromagnetism in $Eu_{2-x}Ce_xRuSr_2Cu_2O_{10-\delta}$ *Ruthenate and Rutheno-Cuprate Material: unconventional superconductivity, magnetism and quantum phase transitions* ed M Cuoco, a Romano (Berlin: Springer) p 142-159.

[21] Hasegawa T, Kishio K, Aoki M, Ooba N, Kitazawa N, Fueki K, Uchida S, Tanaka S 1987 High T_c Superconductivity of $(La_{1-x}Sr_x)_2CuO_4$ –Effect of Substitution of Foreign Ions for Cu and La on Superconductivity *Jpn. J. Appl. Phys.* **26** p L337

[22] Hosoya S, Shamoto S , Onoda M, Sato M 1987 High-T_c Superconductivity in New Oxide Systems II *Jpn. J. Appl. Phys.* **26** p L456

[23] Broun H F, Bauernfeind L, Korf O, Papageorgiou T P 2002 A Phase Diagram Approach to Superconductivity and Magnetism in Rutheno-Cuprates *Ruthenate and Rutheno-Cuprate Material: unconventional superconductivity, magnetism and quantum phase transitions* ed M Cuoco, a Romano (Berlin: Springer) p 118

[24] Bauernfeind L, Widder W, Braun H F 1995 Ruthenium-based layered cuprates $RuSr_2LnCu_2O_8$ and $RuSr_2(Ln_{1+x}Ce_{1-x})Cu_2O_{10}$ (Ln=Sm, Eu and Gd) *Physica C* **254** p 151

[25] Felner I, Asaf I, Levi Y, Millo O 2000 Tuning of the superconducting and ferromagnetic behavior by oxygen and hydrogen in $Eu_{1.5}Ce_{0.5}RuSr_2Cu_2O_{10-\delta}$ *Physica C* **334** p 141

[26] Brown A, Marco S 1942 *Introduction to Heat Transfer* (New York: McGraw-Hill Book Co.) p 8

[27] Berman R 1976 *Thermal Conduction in Solids* (London: Oxford University Press) p 4, p 94

[28] White G K 1979 *Experimental Techniques in Low-Temperature Physics* (New York: Oxford University Press) p 178

[29] Incropera F P, DeWitt D P 1996 *Fundamentals of Heat and Mass Transfer* (New York: John Wiley & Sons) p 47

[30] Lynton E A 1962 *Superconductivity* (New York: John Wiley & Sons) p 136

[31] Kasap S O 2001 *Thermoelectric Effects in Metals: Thermocouples Principles of Electrical Materials and Devices* (New York: McGraw-Hill Book Co.)

[32] Barnard R D 1972 *Thermoelectricity in Metals and Alloys* (London: Taylor & Francis LTD) p 9

[33] MacDonald D K C 1962 *Thermoelectricity: An Introduction to the Principles* (New York: John Wiley & Sons, Inc.)

[34] Kubakaddi S S, Butcher P N, Mulimani B G 1991 Influence of Umklapp process on the sign of phonon-drag thermopower in semiconductor superlattices *J. Phys.:* Condens. Matter **3** p 5445

[35] REEDHOLM 2005 Performing Accurate Low Resistance and Low Voltage Resistance Measurements *Support Notes* http://www.lricks.com/lowresmeas.htm

[36] Dunlap R A 1988 *Experimental Physics* (New York: Oxford University Press) p 150

[37] Bolton W 2004 *Instrumentation and Control Systems* (Oxford: Elsevier) p 82

[38] Awana V P S, Rajeev Ranjan, Rajeev Rawat, Sharath Chandra L S, Peurla M, Ganesan V, Kishan H, Pandey D, Laiho R, Takayama-Muromachi E, and Narlikar A V 2006 Anomalous lattice expansion of $Eu_{1.5}Ce_{0.5}RuSr_2Cu_2O_{10-\delta}$ (Ru-1222) magneto superconductor: A low temperature X-ray diffraction study. *Cond-mat* **10604587** (Accepted in *Physica C*)

[39] Lal R, Awana V P S, Kishan H 2006 Magnetism, upper critical field and thermoelectric power of magneto-superconductor $Eu_{1.5}Ce_{0.5}RuSr_2Cu_2O_{10-\delta}$ *J Phys: Condens. Matter* **18** p 2563L

[40] Lorenz B, Meng R L, Cmaidalka J, Wang Y S, Lenzi J, Xue Y Y, Chu C W 2001 Synthesis, characterization and physical properties of the superconducting ferromagnet $RuSr_2GdCu_2O_8$ *Physica C* **363** p 251

[41] Cardoso C A, Lanfredi J C, Chiquito A J, and Araujo-Moreira F M, Awana V P S, Kishan H, de Almeida R L, de Lima O F Magnetic and superconducting properties of $Gd_{1.5}Ce_{0.5}RuSr_2Cu_2O_{10-\delta}$ samples: dependence on the oxygen content and aging affects *Phys Rev B* **71** p 134509

[42] Belevtsev B I, Hennings B D, Rathnayaka K D D, and Naugle D G 2003 Thermal conductivity in magnetic superconductors **46** ed. A.V. Narlikar (New York: Nova Science Publ.)

[43] Xue Y Y, Lorenz B, Baikalov A, Cao D H, Li Z G, and Chu C W 2002 Superconductivity, intergrain penetration depth, and Meissner effect of $RuSr_2(Gd,Ce)_2Cu_2O_{10-\delta}$ *Phys Rev B* **66** p 0145XX

[44] Felner I, Asaf U, Galstyan E 2002 Magnetic-Superconducting phase-diagram of $Eu_{2-x}Ce_xRuSr_2Cu_2O_{10-\delta}$ *Phys Rev B* **66** p 024503

[45] Felner I 2003 Coexistence of Superconductivity and Magnetism in $R_{2-x}Ce_xRuSr_2Cu_2O_{10-\delta}$ (R=Eu and Gd) *Studies of High Temperature Superconductors* ed V A Narlikar (New York: Nova Science) p 41

[46] Lorenz B, Xue Y Y, and Chu C W 2003 Phase separation, magnetism and superconductivity in rutheno-cuprates *Studies of High Temperature Superconductors* ed V A Narlikar (New York: Nova Science) p 1-39

[47] Felner I, Sonin E B, Machi T, and Koshizuka N 2000 Spontaneous vortex phase and the Meissner-State in the magneto-superconductor $Eu_{1.5}Ce_{0.5}RuSr_2Cu_2O_{10-\delta}$ (Eu-1222) *Physica* C **341-348** p 715

[48] Белевцев Б И 1990 Сверхпроводимость и локализация электронов в неупорядоченных двумерных металлических системах *Успехи Физических Наук* **160** с 65 (Belevtsev B I 1990 Superconductivity and electron localization in disordered 2D-systems *Uspechi* **160** p 65)

[49] Naugle D G, Rathnayaka K D D, Krasovitsky V B, Belevtsev B I, Anatska M P, Agnolet G, Felner I 2006 Transport, thermal, and magnetic properties of $Gd_{1.5}Ce_{0.5}RuSr_2Cu_2O_{10-\delta}$, a magnetic superconductor *Journal of Applied Physics* **99** p 08M501-1

[50] Belevtsev B I, Beliayev E Y, Naugle D G, Rathnayaka K D D, Anatska M P, and Felner I Granular superconductivity in polycrystalline ruthenocuprate $Gd_{1.5}Ce_{0.5}RuSr_2Cu_2O_{10-\delta}$: magnetoresistive and magnetization studies (to be published)

[51] Gonzales G M, Rodrigues-Mijangos R, and Galvan D H 2001 Oxygen-Doping dependence of thermal conductivity measurements in $EuBa_2Cu_3O_{7-\delta}$ *Phys Stat Sol (a)* **184** p 303

[52] Gonzales G M, and Rodrigues-Mijangos R 1999 Oxygen-Doping dependence of thermoelectric power and thermal conductivity measurements in $EuBa_2Cu_3O_{7-\delta}$ International Journal of Modern Physics B **13** p 3663

[53] Popoviciu C P and Cohn J L 1997 Thermal transport in $YBa_2Cu_3O_{6+x}$: Doping dependence across the phase diagram *Phys Rev B* **55** p 3155

[54] Liang W Y 1998 Are high-T_c cuprates unusual metals? *J Phys: Condens. Matter* p 11365

[55] Obertelly S D, Cooper J R, Tallon J L 1992 Systematics in the thermoelectric power of high-T_c oxides *Phys Rev B* **46** p 14928

[56] Trodahl H J 1995 Thermopower of the superconducting cuprates *Phys Rev B* **51** p 6175

[57] Blatt F J, Schroeder P A, Foiles C L, and Greig D 1977 *Thermoelectric Power of Metals* (New York: Plenum Press)

[58] Choi M Y (Mu-Yong), Kim J S 1999 Thermopower of high-T_c cuprates *Phys Rev B* **59** p 000192

[59] Awana V P S 2005 Magneto-Superconductivity of rutheno-cuprates *Frontiers in Magnetic Materials* ed A V Narlikar (Germany: Springer-Verlag) p 531

[60] Cohn J L, Kowe-Ma C K, Vanderah 1995 Anomalous phonon damping and thermal conductivity in insulating cuprates *Phys Rev B* **52** p R13134

VITA

Name: Maryna Petrovna Anatska

Address: Texas A&M University, Department of Physics, College Station, TX 77843-4242

Email Address: manatska@physics.tamu.edu

Education: B.A., Physics, Belarusian State University at Minsk, Belarus, 1999
M.S., Physics, Texas A&M University at College Station, Texas, 2006